



Investigations into a Dynamic Datum for California

Yehuda Bock and Emilie Klein

June 22, 2018

Per Interagency Agreement 52A0103

Regents of University of California and California Department of Transportation
and

Scripps Institution of Oceanography (SIO)

Copyright © 2018 California Department of Transportation
All Rights Reserved

The California Department of Transportation (Caltrans), grants UCSD/SIO/CSRC a non-exclusive, royalty-free license to use, reproduce, publish and disseminate the Report titled "Investigations into a Dynamic Datum for California" in any form and format, solely for the purpose necessary to fulfill its mission of research, education, and public service and for noncommercial and/or profit.

Summary

Maintenance of a fixed geodetic datum is complicated by California's crust being subject to a variety of motions at different spatial and temporal scales. The motions are the result of tectonic and magmatic processes and vertical land motion due to natural (e.g., drought) and/or anthropogenic effects (e.g., water and mineral extraction). To address this difficulty the California Spatial Reference Center (CSRC) has published five "Epoch Date" datums since 2002, as a realization of a California Spatial Reference System (CSRS). The latest is "CSRS Epoch 2017.50 (NAD83)," for short "Epoch 2017.50," defined by the geodetic coordinates and uncertainties of the 948 California Spatial Reference Network (CSRN) stations (839 active and 109 defunct) (http://csrc.ucsd.edu/CSRC_Epoch2017_50.shtml) at 2017.50 (July 2, 2017).

Epoch 2017.50 is aligned with the current definition of the National Spatial Reference System (NSRS) through a set of coordinate transformations from ITRF2014 to NAD83(2011), published by the NOAA/NOS National Geodetic Survey (NGS). The NGS, as part of its mission, is required to define, maintain and provide access to the NSRS. The NGS will replace NAD83 with the new geometric reference frame in 2022. The North American Terrestrial Reference Frame of 2022 (NATRF 2022) will cover North America and includes the Continental United States (CONUS). It will be a "plate fixed" system similarly based upon the IGS realization of ITRF2014, with the application of rotations about a Euler Pole to remain closely anchored to the North American tectonic plate. However, the extreme western portions of CONUS are not on the North American plate and experience significant motions that need to be considered as a supplement to the 2022 update. The NOAA Technical Report NOS NGS 62, 2017 "Blueprint for 2022, Part 1: Geometric Coordinates" acknowledges the need for a supplemental Intra-Frame Velocity Model (IFVM) for the "Intra-Plate zones" but leaves undefined how this might be developed, funded or implemented.

This task order is to consider a conceptual plan for a Pilot Dynamic Datum demonstration. This datum could replace the Epoch Date approach and allow a seamless and continuous tie to NATRF 2022. Our study indicates that a dynamic datum can be successfully implemented in California and therefore across the North American-Pacific intra-plate zone. This report presents a methodology to do so. We used the Epoch 2017.50 displacement data set, available from Task 2 of Caltrans/SIO Agreement Number 52A013, as a convenient test bed for the study.

According to our task plan, we have addressed how to:

- (1) Define the process and resources required to enhance the NGS modeling utility, Horizontal Time Dependent Positioning (HTDP), if available, or to develop a new modeling utility for the geophysically-complex area of California.
- (2) Determine the appropriate resolution of the grid files needed to accurately interpolate secular velocities over time, forward and backwards, as a comparison to (1). The test bed includes the horizontal velocity vectors from the publication of Epoch 2017.50 for the years 2010.00 to 2017.9.
- (3) Develop a conceptual plan for addressing and updating the model to incorporate displacements associated with earthquakes and other sources of ground motions, as needed.
- (4) Identify and propose potential collaborative partners and stakeholders that would benefit from the development of this utility and could participate in, or contribute to the development, including potential funding partners. This should include partners in western CONUS outside of California.
- (5) Collaborate with NGS through the Pacific Southwest Regional Advisor, together with the Southwest and recently-installed Northwest Regional Advisors, on the development of this conceptual plan.
- (6) Develop a QA/QC plan for testing the accuracy and reliability of the Pilot Project model.

Contents

Summary.....	2
1. Background.....	4
2. Methodology	6
2.1 GNSS data analysis.....	7
2.2 Time series analysis.....	7
2.3 Elements of a dynamic datum.....	10
2.4 Surface displacement grids	13
Horizontal datum	13
Vertical datum	17
3. Discussion	21
4. Implementation	22
4.1 Post-Processing.....	23
4.2 Real-Time Surveying.....	23
4.3 HTDP software	24
5. QA/QC Plan	25
6. Recommendations	25
Acknowledgments	26
References	27
Displacement Grid Movies.....	29
List of Acronyms	29

1. Background

In 2022 the National Geodetic Survey (NGS) will publish a new geometric reference frame for CONUS and other regions (<https://www.ngs.noaa.gov/datums/newdatums/index.shtml>) that will redefine and update the National Spatial Reference System (NSRS). The North American Terrestrial Reference Frame of 2022 (NATRF 2022) will provide a plate-fixed reference frame anchored to the considered stable North American tectonic plate through the application of rotations about a Euler Pole west of the Galapagos Islands. However, the extreme western portions of CONUS are not on the North American plate. Western CONUS is subject to a variety of motions at various spatial and temporal scales that complicate the maintenance of a fixed geodetic datum and its tie to NATRF 2022. Secular (steady) motions are the result of tectonic processes that cause primarily horizontal motions in strike-slip environments such as the San Andreas fault, with some vertical motions in thrust fault environments such as the Cascadia subduction zone. The North American-Pacific Plate boundary runs along the primarily right-lateral strike-slip San Andreas Fault system from Southern California northwesterly, approaching the Pacific coast in the San Francisco Bay Area and continuing along the coast to Cape Mendocino. In this region, the Pacific Plate is moving northwesterly, relative to the North American Plate, at velocities approaching 5 centimeters (~2 inches) per year (Figure 1). North of the Cape Mendocino area and extending to Western Canada is the Cascadia subduction zone with complex deformation of comparable magnitudes. The steady secular motions are punctuated by earthquakes that cause significant coseismic and non-linear postseismic displacements (Table 1).

Non-secular vertical land motions are also present throughout California, primarily due to magmatic processes, for example, the Long Valley caldera at Mammoth Lakes, water aquifer recharge, anthropogenic sources, including water and mineral extraction, and hydrothermal power plants, and natural causes such as hydrological

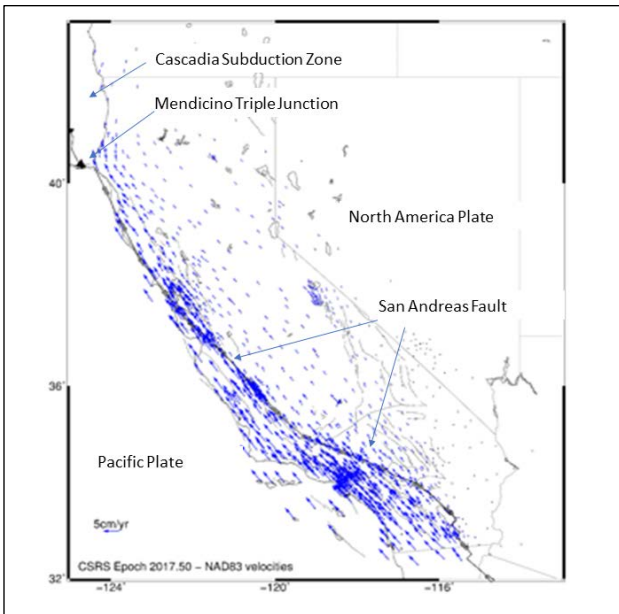


Figure 1. Horizontal station velocities. Estimated velocities with respect to North America Datum 1983 (NAD83) as part of the Epoch 2017.50 adjustment, for 948 California Spatial Reference Network (CSRN) stations.

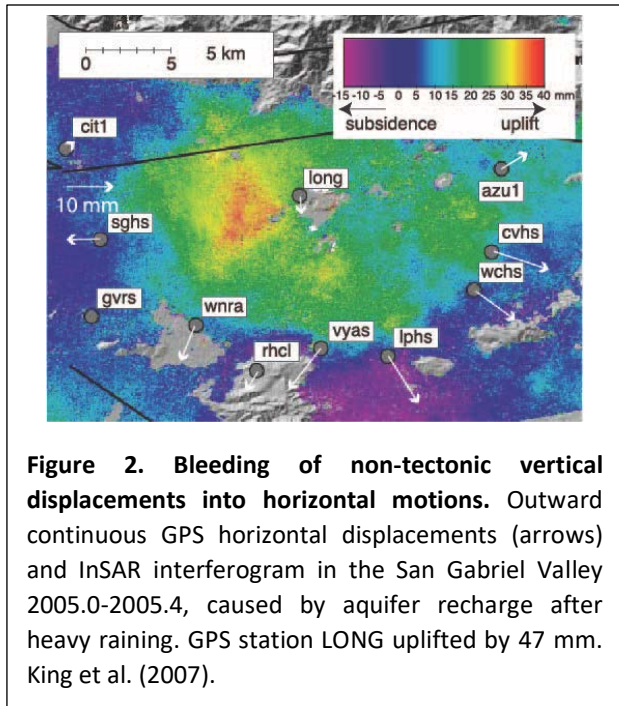


Figure 2. Bleeding of non-tectonic vertical displacements into horizontal motions. Outward continuous GPS horizontal displacements (arrows) and InSAR interferogram in the San Gabriel Valley 2005.0-2005.4, caused by aquifer recharge after heavy raining. GPS station LONG uplifted by 47 mm. King et al. (2007).

surface loading. Crustal deformation models are often complicated by these non-tectonic processes that cause primarily vertical land motion (subsidence and uplift) but can also bleed into horizontal motions (Figure 2) (King et al. 2007), complicating the maintenance of a horizontal datum. California has experienced rapid subsidence in the Central Valley, bounded by the Sierra Nevada range to the east and the Coast ranges to the west, with an area of about 10,000 square miles. Here, groundwater extraction for agricultural development began in the 1920's. Since then, three severe droughts, the last between 2013 and 2016, contributed to more than a meter of subsidence. The Central Valley, lying on an aquifer, responds to hydrological poroelastic processes. When groundwater is extracted, downward motion due to soil compaction is observed. Additionally, daily position time series of GNSS stations show vertical land motion due to the solid Earth's elastic response to the loading and unloading of snow and surface water (Argus et al., 2014; Amos et al., 2014) and drought (Borsa et al., 2014). Although GNSS networks located to monitor tectonic deformation seek to avoid placing stations atop aquifers, this is often not possible because large basins in developed areas often intersect tectonically active regions. This is a significant problem in California in areas such as the Los Angeles (e.g., Bawden et al., 2001) and Santa Maria basins (King et al., 2007).

To mitigate the positional degradation over time, we propose the implementation of a dynamic geodetic datum through a combination of observed surface displacements and underlying geophysical models. The Pilot Project scoped under this task order would include the further development and testing of our proposed methodology.

Note that we use "GNSS" in this report unless it is more appropriate to use "GPS," when only GPS observations were used.

Table 1. Significant earthquakes affecting California 1992-2018

Date	UTC	Name	Mw	Depth	Latitude (N)	Longitude (W)	Stations Affected
6/28/1992	11:57:34	Landers	7.3	1.1	34.217	116.433	5
10/16/1999	9:46:44	Hector Mine	7.1	20	34.54	116.267	163
12/12/2003	19:15:56	San Simeon	6.5	7.6	35.706	121.102	23
9/28/2004	17:15:24	Parkfield	6.0	7.9	35.815	120.374	28
6/15/2005	2:50:54	Gorda Plate	7.2	10	41.284	125.983	7
6/17/2005	6:21:41	Off the Coast N. California	6.7	10	40.758	126.595	7
9/2/2005	1:27:19	Obsidian Buttes Swarm	5.1		33.16N	115.637	3
10/31/2007	3:04:55	Alum Rock	5.6	9	37.432	121.776	1
7/29/2008	18:42:15	Chino Hills	5.5	14.7	33.95	117.76	1
1/10/2010	0:27:39	Eureka, Offshore N. California	6.5	29.3	40.652	124.692	11
4/4/2010	22:40:43	El Mayor-Cucapah, Mexico	7.2	10	32.259	115.287	221
6/15/2010	4:26:59	Aftershock, El Mayor-Cucapah	5.7		32.698	115.924	7
7/7/2010	23:53:33	Borrego Springs	5.4		33.417	116.483	3
8/26/2012	19:31:22	Brawley Seismic Swarm	5.3, 5.4	9.2	33.019	115.546	4
10/21/2012	6:55:09	Central California	5.3		36.31	120.856	4
3/10/2014	5:18:13	Offshore Ferndale	6.8	7	40.821	125.1277	18
3/30/2014	4:09:42	La Habra, NW Orange County	5.1	7.5	33.92	117.940	1
8/24/2014	10:20:44	South Napa	6.1	10.7	38.215	122.318	16

2. Methodology

The objective is to provide a dynamic datum modeling utility for surveying and precise spatial referencing within an active tectonic area such as western CONUS spanned by a dense cGNSS reference network. This would allow for the transformation of coordinates from one date to another, without the need for periodic Epoch Date definitions, such as Epochs 2011.00 and 2017.50. A key component is an underlying observation and analysis infrastructure to precisely estimate changes in position for the reference stations. The estimated positions form a time series of displacements with respect to an initial epoch. The resulting displacement time series are parametrically modeled for station velocities and coseismic and postseismic motions. All observations and calculations are performed within the ITRF system simplifying the transformations to modernized NATRF 2022 and North American-Pacific Geopotential Datum of 2022 (NAPGD 2022), as well as legacy NAD83 datums

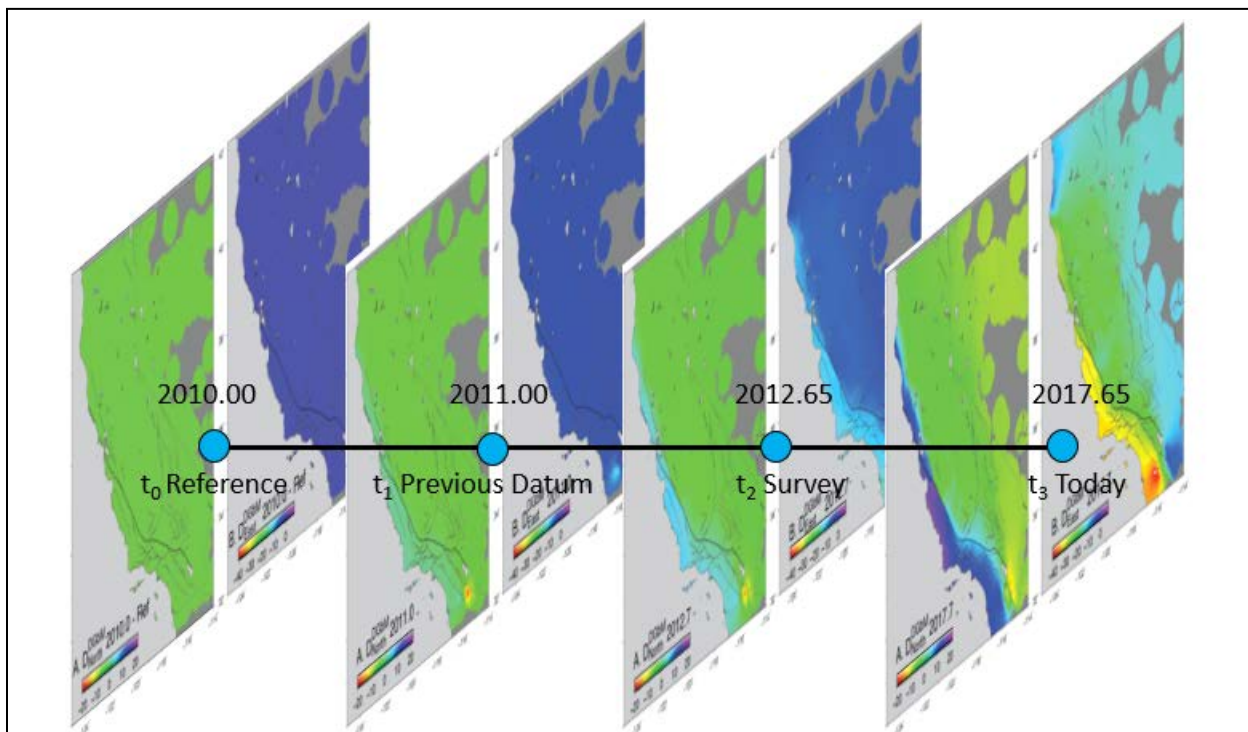


Figure 3. Concept of a dynamic datum. Transformation of station coordinates for two separate surveys to Epoch 2011.00, one with true-of-date RTK surveying ($t_3=2017.65$) and one in post-processing ($t_2=2012.65$). Best practices call for positioning with respect to the latest version of ITRF (ITRF2014), which is consistent with the GNSS broadcast ephemerides and published ultra-precise and final IGS orbits. The dynamic datum allows the coordinates at t_3 and t_2 to be transformed to an arbitrary epoch t_1 , still in ITRF, using archived coordinate correction grids updated weekly at SOPAC. The coordinates can then be transformed to NAD83, or other datum of choice at t_3 and t_2 . Epoch t_0 refers to the start of the daily displacements time series.

(<https://www.ngs.noaa.gov/datums/newdatums/naming-convention.shtml>).

In this report “true-of-date” coordinates refer to the coordinates of a station on a specific date as derived from a time series of GNSS-derived displacements (section 2.2). This is the basis of SOPAC’s SECTOR utility (<http://sopac.ucsd.edu/sector.shtml>). However, SECTOR is only valid for the reference network and not for any arbitrary location within the area of interest. A dynamic datum requires a further correction to account for the expected displacements of survey stations between any two dates due to tectonic and

other motions. A correction is required to transform true-of-date station positions to any other arbitrary date (Figure 3). For this study, we make use of the daily displacement time series from the Epoch 2017.50 project, consisting of 948 California Spatial Reference Network (CSRN) stations (839 active and 109 defunct) (http://csrc.ucsd.edu/CSRC_Epoch2017_50.shtml).

2.1 GNSS data analysis

The basic GNSS observables are multiple-frequency phases and pseudoranges collected from available satellites, stored in 24-hour RINEX files sampled at a rate of 15 seconds. For Epoch Date 2017.50, we used RINEX files for global and regional reference stations and associated metadata (e.g., antenna heights and antenna models) gathered from the SOPAC archive (garner.ucsd.edu). The global stations are required to estimate GNSS satellite orbits and earth orientation parameters (EOP - polar motion and variations in the Earth's rotation rate). We used the GAMIT/GLOBK software (<http://www-gpsg.mit.edu/~simon/gtgk/>; Herring et al., 2008) in network positioning mode, resulting in daily GAMIT “h-files” containing unconstrained global geocentric Cartesian ITRF2014 (X,Y,Z) station coordinates and their corresponding covariance matrices. For Epoch 2017.50 analysis, we used data from ~300 global stations. The global and regional h-files were adjusted by the GLOBK software and nominally aligned to ITRF2014 using the IGS realization of this frame (IGS14), which currently is based on 113 global stations. The (X,Y,Z) coordinates of the California reference stations were converted to displacements in North, East and Up directions (ΔN , ΔE , ΔU) relative to the (X,Y,Z) coordinates at the first time series epoch for a station, using the geodetic latitude and longitude of the station (ϕ , λ). The output is called the “raw daily displacement time series.” After gross outliers are removed, the output is called the “cleaned daily displacement time series.”

2.2 Time series analysis

The time series analysis of daily displacements can be performed component by component since the correlations between (ΔN , ΔE , ΔU) components are small (Zhang 1996). The displacement time series are analyzed using JPL's `analyz_tseri` software (<https://qoca.jpl.nasa.gov/>) according to the parametric model of Nikolaidis (2002), except for a modified annual and semiannual parameterization, such that

$$y(t_i) = a(t_0) + bt_i + c [\sin(\omega t_i + \varphi_d)] + e [\sin(2\omega t_i + \varphi_f)] + \sum_{j=1}^{n_g} g_j H(t_i - T_{g_j}) + \sum_{j=1}^{n_h} h_j H(t_i - T_{h_j}) t_i + \sum_{j=1}^{n_k} k_j e^{\left[1 - \left(\frac{t_i - T_{k_j}}{\tau_j}\right)\right]} H(t_i - T_{k_j}) + \varepsilon_i \quad (1)$$

The coefficient a is the value at the initial epoch t_0 (“y-intercept”) and t_i denotes the time elapsed from t_0 in units of years. The linear rate (slope) b represents the interseismic (secular) tectonic velocity, expressed in mm/yr. The coefficients c , φ_d , e , φ_f are the amplitude (mm) and phase (degrees) of annual and semi-annual variations, respectively. The coefficients g_j represent n_g possible offsets (mm) due coseismic deformation and non-coseismic changes at respective epochs T_{g_j} . Most non-coseismic offsets are due to the replacement of GNSS antennas with different phase center characteristics but can also be related to changes in the station environment due, for example, to tree trimming. Possible n_h changes in velocity are denoted by new velocity values h at respective epochs T_{h_j} . In this study, we only assign a single velocity per station. Postseismic coefficients k are for n_k postseismic motion events starting at epochs T_{h_j} and either decaying exponentially with a time constant τ_j , as in the last term of Equation 1, or logarithmically according to

$$\sum_{j=1}^{n_k} k_j \log \left(1 + \frac{t_i - T_{k_j}}{\tau_j} \right) H(t_i - T_{k_j}) \quad (2)$$

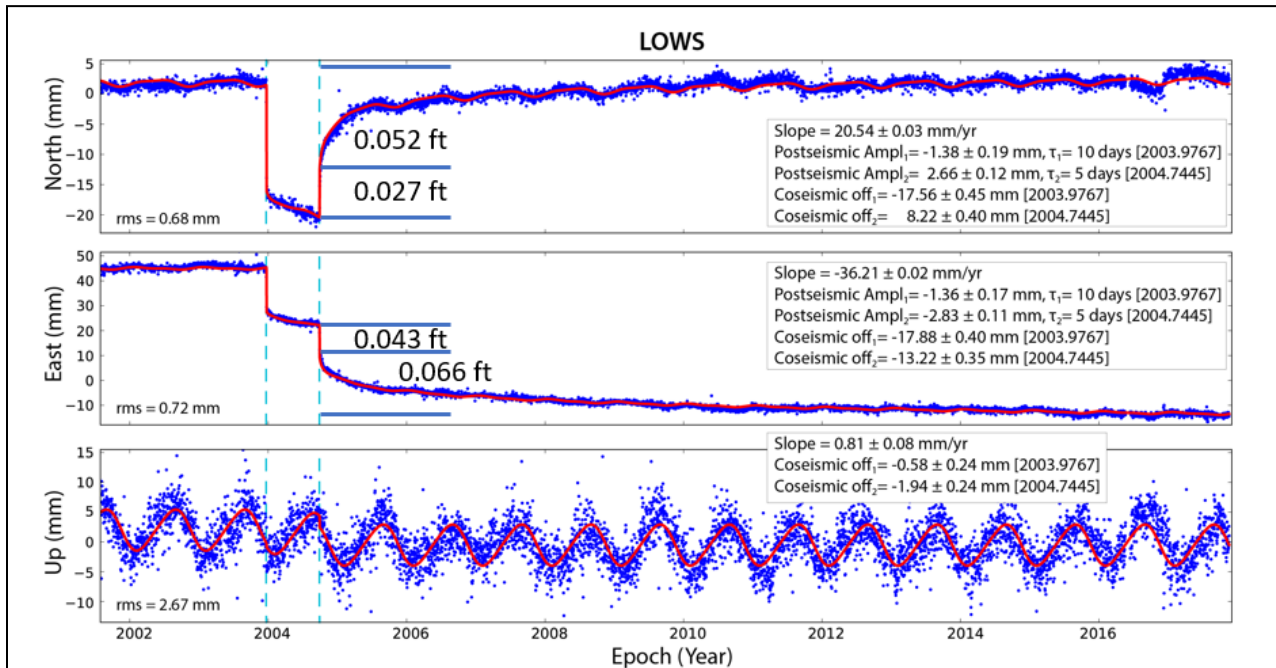


Figure 4. Relative magnitudes of coseismic and postseismic deformation. Displacement time series (blue dots, SOPAC daily processing) of the station LOWS (35.829°N, 120.594°W) near Parkfield, Central California, showing coseismic and postseismic displacements due to the 2003 Mw6.6 San Simeon and 2004 Mw6.0 Parkfield earthquakes (Table 1). The red curve depicts the time series model (Equation 1). For the Parkfield earthquake, the coseismic displacements are 0.027 ft and 0.043 ft for the north and east components, respectively, while the corresponding cumulative postseismic displacements through to 2017 are 0.052 ft. and 0.066 ft.

The choice of postseismic model is based on the characteristics of the earthquake and the response of the Earth’s crust. [Note: The exponential model is often associated with viscoelastic relaxation in the upper mantle (see Figure 8) and has been applied to, for example, the 1992 Mw7.3 Landers, California earthquake (Shen et al. 1994). The logarithmic model is associated with afterslip on the fault surface, and was applied, for example, to the 2004 Mw6.0 Parkfield, California earthquake (Freed 2007)].

As a preliminary step, the non-linear postseismic decay τ_j is estimated by a maximum likelihood method as described by Nikolaidis (2002). Then fixing the parameters τ_j , the other parameters (a-h) in Equation 1 are estimated by linear least squares, resulting in the “modeled daily displacement time series” (Figure 4).

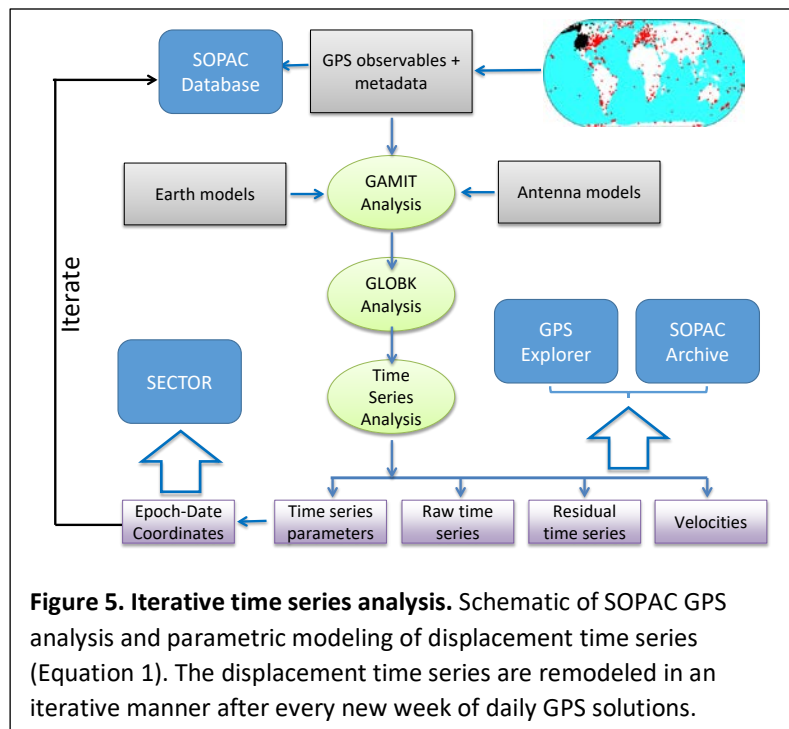
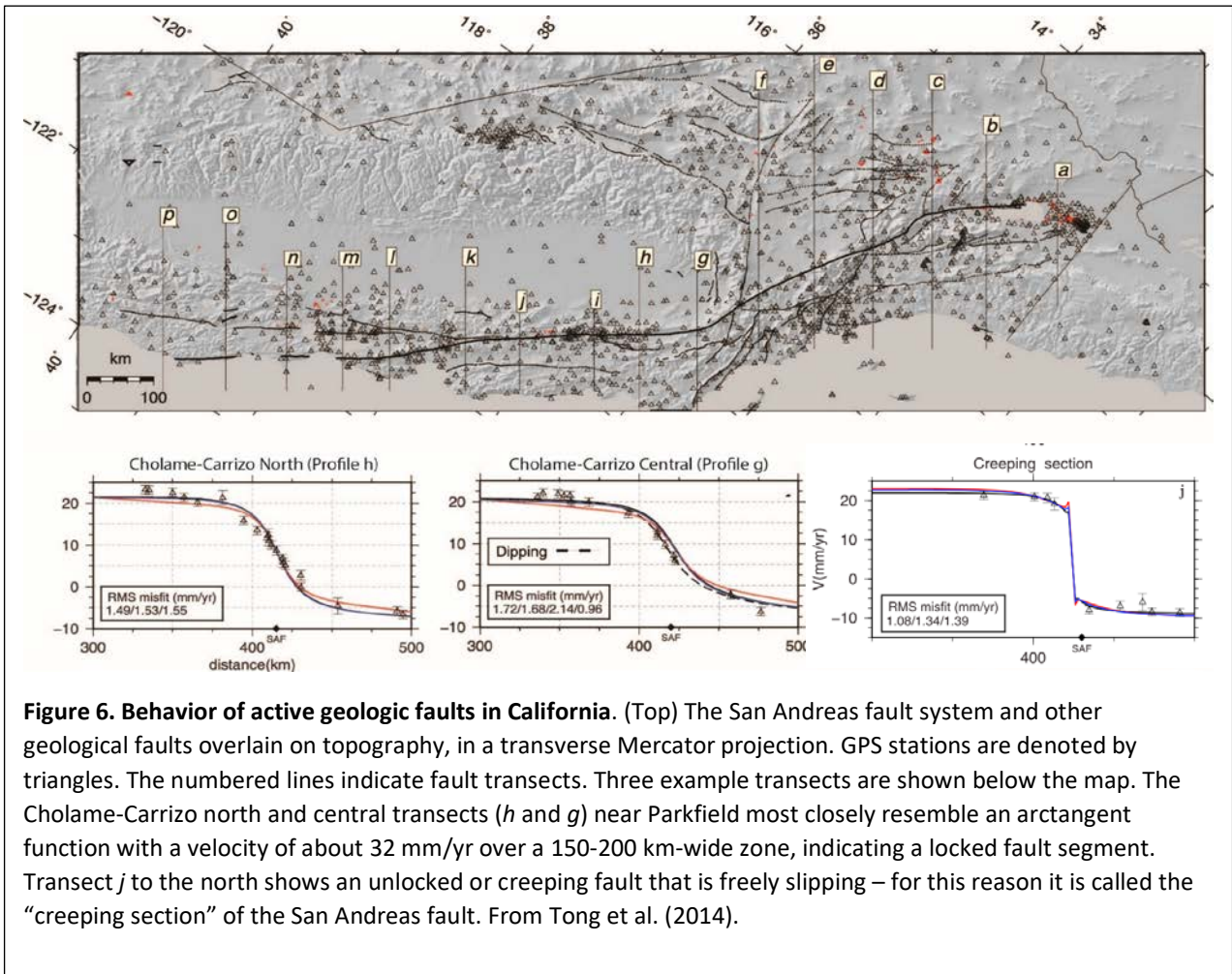


Figure 5. Iterative time series analysis. Schematic of SOPAC GPS analysis and parametric modeling of displacement time series (Equation 1). The displacement time series are remodeled in an iterative manner after every new week of daily GPS solutions.

The residuals of this process denote the deviations from the time series model (Equation 1). The uncertainties of the velocity parameters are scaled to account for colored (time-dependent) noise observed in the displacement time series according the approximate expression of Williams (2003).

In SOPAC’s operational analysis the raw displacement time series are extended each week with seven daily solutions (Figure 5). Then, the parametric parameters (a-h) of the extended time series (some as early as 1995) are re-estimated to maintain a consistent long-term data record. The “true of date” coordinates seed the next week’s GAMIT/GLOBK analysis. The same frame is then used to generate the next set of satellite orbits and EOPs using the updated (modeled) true-of-date coordinates, and so on. We still maintain a loose connection to ITRF through the GLOBK analysis. This iterative process includes an analysis of all the position data to date, validation of relevant metadata, automatic and manual quality control for the individual time series, identification of instrumental offsets, appropriate fitting/modeling of the time series and an administrator web interface to perform detailed quality control and to improve the position time series models. This approach is taken to best account for seismic events with significant coseismic and postseismic motions and other non-tectonic offsets. This dynamic approach can be continued indefinitely. It does not depend on a static list of stations and can accommodate the attrition of stations or the addition of new ones. In practice, the SOPAC analysis is combined with an independent analysis, of the same data and metadata, by the Jet Propulsion Laboratory (JPL) Bock et al., 2016) (<http://garner.ucsd.edu/pub/timeseries/measures/ats/WesternNorthAmerica/>).



2.3 Elements of a dynamic datum

The need for a dynamic geodetic datum can be stated as follows (Figure 3). A surveyor requires knowledge of the motions of an arbitrary station to seamlessly transform coordinates between any two dates. For example, for a survey taken at 2017.65 the station coordinates may need to be transformed to 2011.00 (the CSRS Epoch Date prior to 2017.50) to be consistent with the organization’s geographical information system (GIS).

We make use of two sources of information. The first source is the directly observed daily displacement time series from the network of reference stations. For this study we use the SOPAC time series from the Epoch 2017.50

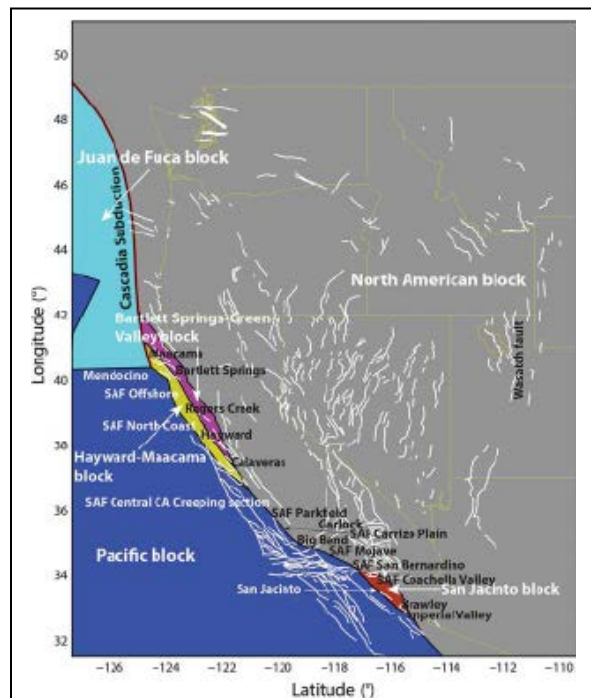


Figure 7. Block model of Western CONUS. The geophysical model used for our study is based on the division of the region into distinct physical blocks (Zeng and Shen, 2017).

project, consisting of 948 CSRN stations (839 active and 109 defunct). For the dynamic datum, we need to correct the displacement time series for non-tectonic offsets but retain the coseismic offsets. Therefore, using the estimated parameters from the time series analysis we correct the input time series for all the offsets (coefficients “g” in Equation 1) and re-inject the estimated coseismic offsets. Now, the station displacements represent the physical motions of the stations. Although the annual and semi-annual terms may contain some artifacts external to the reference network, we assume that these are purely physical motions within the region.

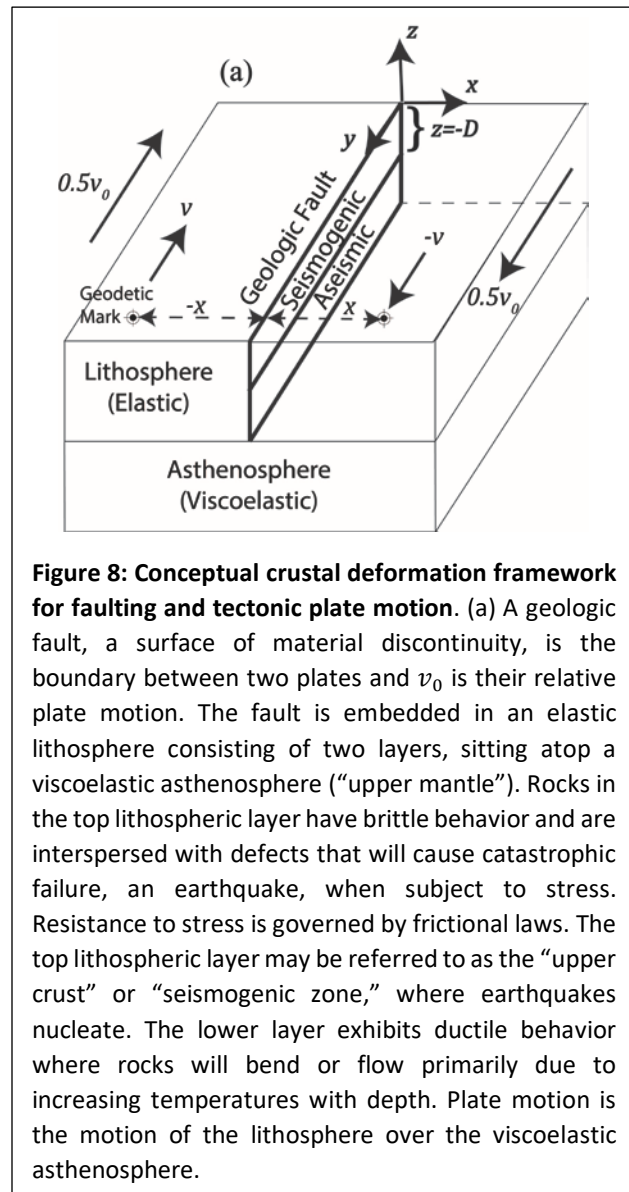
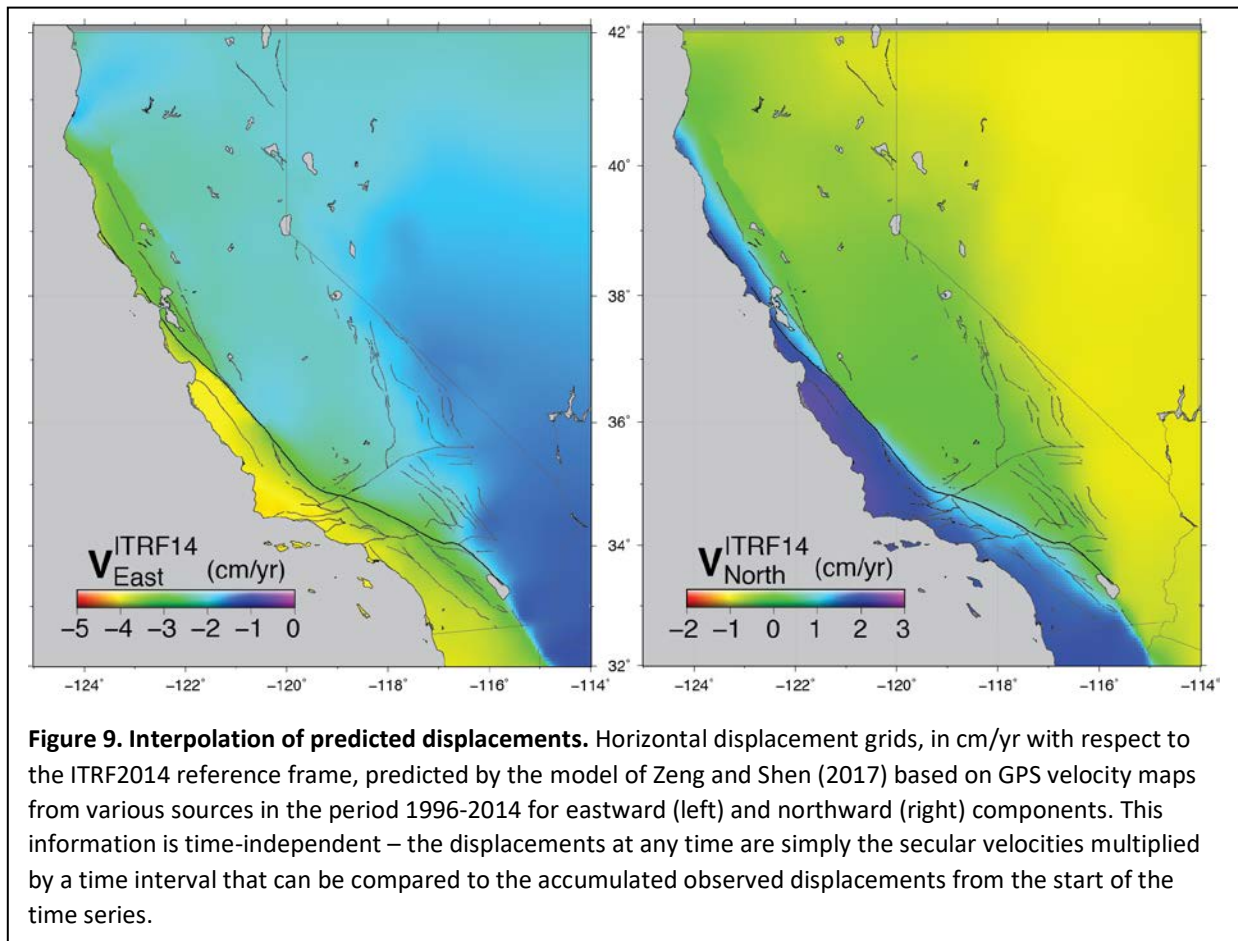


Figure 8: Conceptual crustal deformation framework for faulting and tectonic plate motion. (a) A geologic fault, a surface of material discontinuity, is the boundary between two plates and v_0 is their relative plate motion. The fault is embedded in an elastic lithosphere consisting of two layers, sitting atop a viscoelastic asthenosphere (“upper mantle”). Rocks in the top lithospheric layer have brittle behavior and are interspersed with defects that will cause catastrophic failure, an earthquake, when subject to stress. Resistance to stress is governed by frictional laws. The top lithospheric layer may be referred to as the “upper crust” or “seismogenic zone,” where earthquakes nucleate. The lower layer exhibits ductile behavior where rocks will bend or flow primarily due to increasing temperatures with depth. Plate motion is the motion of the lithosphere over the viscoelastic asthenosphere.

The second source of information is an underlying geophysical model that predicts the surface displacements at the reference stations. A geophysical model contains information on the fault geometries, depths and slip rates (the amount of motion on each fault segment), based on geodetic, geological and seismological observations and assumptions on crustal properties (Bock and Melgar, 2016). The model predicts the expected motions at any point within the region spanned by the reference network (in our study this includes California and its borders with Baja California, Mexico, Arizona, Nevada and Oregon), at any point in time. As new observations and new physical insights become available geophysical models evolve. However, there are different geophysical models published for the same regions. For example, Tong et al. (2014) published a model for the San Andreas fault system (Figure 6), while Zeng and Shen (2017) published a model for the entire Western U.S. (Figure 7). To complicate matters, the methodology for developing these models is subjective and non-unique, which complicates probabilistic earthquake forecasting. Nevertheless, the choice of a model is somewhat arbitrary and a minor issue for the dynamic datum since any reasonable fault model will provide a good starting point to compare with the observed motions. We are primarily concerned with the differences between the observed and predicted displacements.



It is important to explain why a geophysical model is useful. As shown in Figure 6, fault slip at depth manifests itself as surface displacements orthogonal to the fault trace that resemble an inverse tangent function for a locked fault (see transects g and h) or as a step function (transect j) for a creeping fault.

Sections where the fault is creeping, which means that it is freely slipping rather than locked (Figure 6 – profile *j* ‘Creeping section’), we observe a clear offset between both sides of the fault. On the contrary, wherever the fault is not slipping freely and is locked, we observe a slope depending on fault rate. Moreover, this slip decreases with distance away from the fault, up to a width of several hundred kilometers. Such motions near the faults are difficult to capture through interpolation of surface displacements alone. The underlying geophysical model provides predictions of displacements that consider the distribution and movements of the faults, which can be compared to the observed displacements.

Today, most published geophysical models assume that the Earth’s crust behaves as an elastic body. Viscoelastic effects that are important in modeling postseismic deformation are often ignored (Figure 8). Input to these models are horizontal surface velocities estimated from geodetic velocity maps, primarily GNSS. The assumption is that the velocities are secular (steady), and hence time-independent. For this study, we use the model of Zeng and Shen (2017) for Western CONUS, which is derived from horizontal GPS velocity maps collected from numerous sources. A grid based on the interpolation of predicted horizontal displacements is shown in Figure 9 with a resolution of 0.05 degrees (~5.6x5.6 km²). We compute, for each of the reference (CSRN) stations, the observed SOPAC minus the predicted (Zeng and Shen, 2017) (O-P) displacements, for example over the period 2010-2014.6 (Figure 10). The O-P displacements show significant differences due to ongoing postseismic deformation from the 2004 Mw6.0 Parkfield, 2010 Mw7.2 El Mayor-Cucapah and 2014 Mw6.1 South Napa earthquakes (Table 1) and magmatic-induced motions at Long Valley Caldera. Additional differences are due to motions along the “creeping” segment of the San Andreas fault (Figure 6). These are all due to time-dependent phenomena that are not predicted by the elastic model (Zeng and Shen, 2017) but are tracked by the geodetically-observed daily displacement time series. Furthermore, Figure 10 shows significant eastward-pointing vectors due to subduction along the Cascadia subduction zone in northern California. These could be a combination of time-dependent motions or due to the use of a simplified (block) model (Figure 7) for such a complex region.

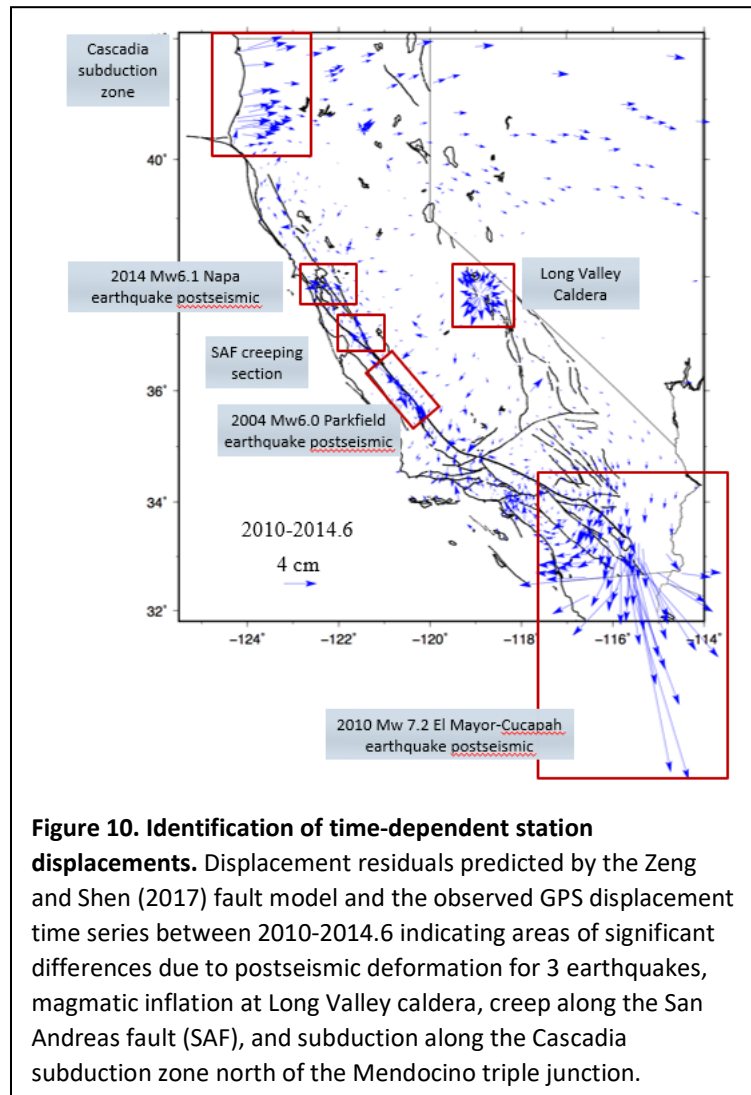


Figure 10. Identification of time-dependent station displacements. Displacement residuals predicted by the Zeng and Shen (2017) fault model and the observed GPS displacement time series between 2010-2014.6 indicating areas of significant differences due to postseismic deformation for 3 earthquakes, magmatic inflation at Long Valley caldera, creep along the San Andreas fault (SAF), and subduction along the Cascadia subduction zone north of the Mendocino triple junction.

2.4 Surface displacement grids

For this study, the vertical is treated differently than the horizontal. For the horizontal dynamic datum, we use both the observed GNSS displacements and the predicted model displacements to create surface motion grids over time. For the vertical datum we only use the observed displacements because vertical motion is more difficult to model.

Considering that we do not require a temporal resolution as fine as one day (the typical analysis frequency) for characterizing the expected motions, for this study the daily displacements are down sampled into a time series of weekly median values for each component (north, east and up) (this is performed with the Generic Mapping Tools (GMT) software's filter1d function). Note that when stations stop recording for several weeks or more (for maintenance or malfunction), they temporarily disappear from the process. We do not interpolate over the missing epochs so as not to bias the predicted station positions and possibly contaminate the grid.

Horizontal datum

Using the geophysical model of Zeng and Shen (2017), we create weekly grids of predicted horizontal displacements accumulated since the reference epoch t_0 , the starting date of the time series. We first compare the observed and predicted reference station displacements, for example the period 2010.0 to 2017.7 (Figure 11A) and difference them to obtain the O-P residual (point) displacements (Figure 11B). We interpolate the point residuals to obtain the O-P displacement grids (Figure 11C) using the *gpsgridded* function of the mapping software GMT5 (Sandwell and Smith, 2016), which assumes that the Earth's crust acts as a 2-D elastic body. The O-P displacement point residuals and grids reflect the effects of time-dependent motions, as well as limitations in the underlying geophysical model.

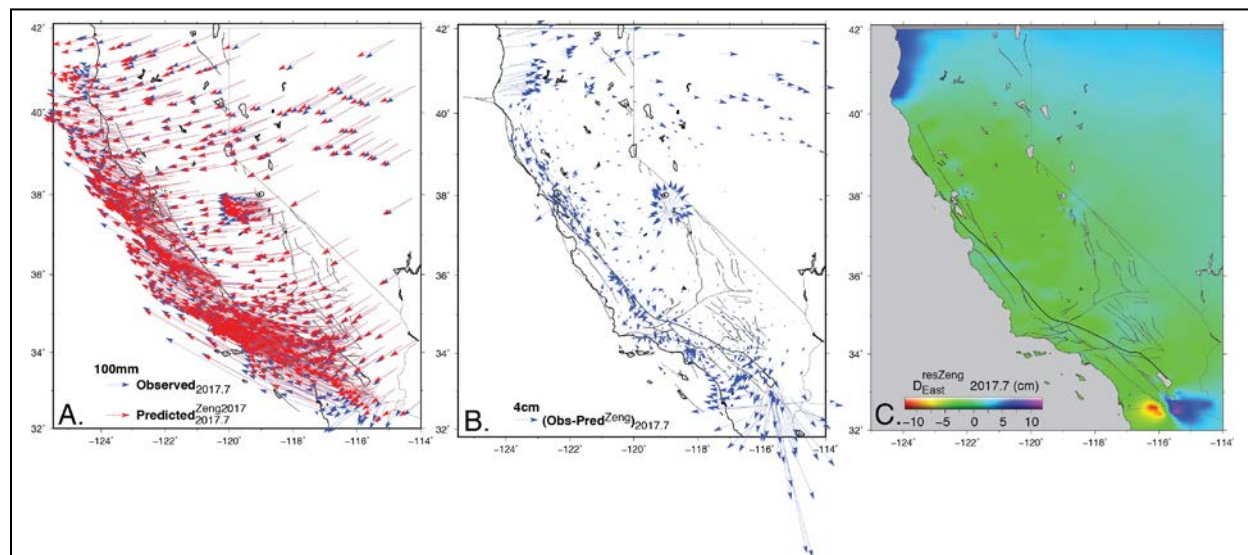


Figure 11. Observed minus predicted (O-P) displacements. East component from 2010.0 and 2017.7. A) SOPAC observed point displacements (blue arrows) and Zeng and Shen (2017) predicted displacements (red arrows) at the reference stations; B) O-P residual motions at the reference stations; C) O-P displacements grid.

The first weekly grid of residuals is added to the corresponding predicted weekly grid from the geophysical model, which defines the Dynamic Geophysical-based Model grid at epoch t_0 , DGbM₀. By the end of the second week, we create a new grid of the accumulated predicted and residual displacements over the last two weeks of observations, and so on. The grids are stored and numbered according to week number t_0 , t_1 , t_2 , etc., where $t_0=2010.0192$, $t_1=2010.0383$, $t_2=2010.0575$ (time in decimal years). For our test data set,

not all stations were operational at the fixed reference date 2010.0. For these stations, the reference date for the estimation of cumulative O-P displacements is the first epoch of their time series. Then, we use the DGBM grid at the date preceding the date of appearance of stations to predict their positions relative to the dynamic datum reference date. At each following epoch (week), the positions of new stations are thus the prediction at their date of appearance plus the measured cumulative displacement, and so on.

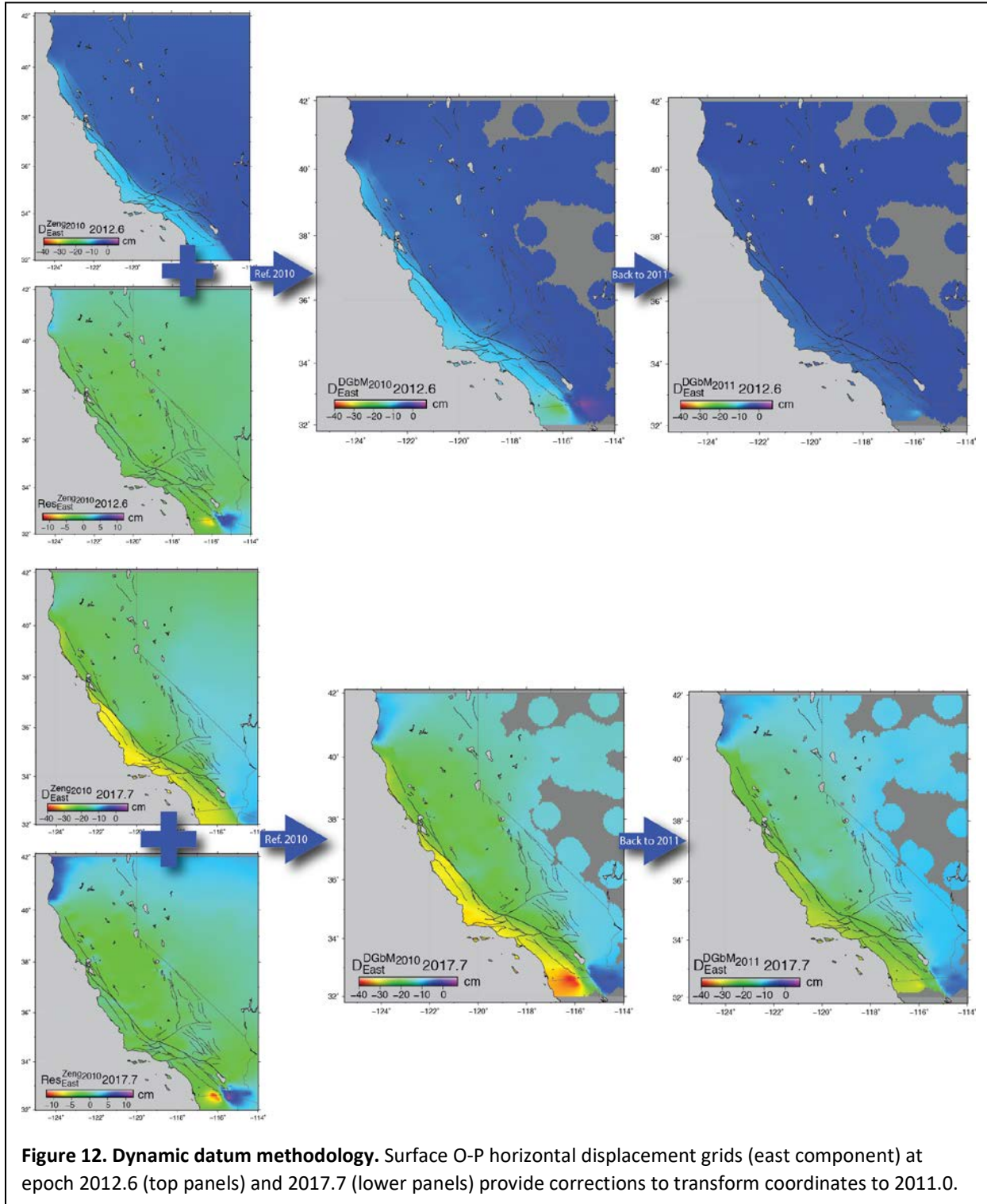


Figure 12. Dynamic datum methodology. Surface O-P horizontal displacement grids (east component) at epoch 2012.6 (top panels) and 2017.7 (lower panels) provide corrections to transform coordinates to 2011.0.

Suppose that a point is surveyed at epoch t_n and we would like to transform its coordinates back to epoch t_m . The grid correction is then $DG\text{bM}_m - DG\text{bM}_n$, where $DG\text{bM}_m$ contains the accumulated displacements from t_0 to t_m and $DG\text{bM}_n$ contains the accumulated displacements from t_0 to t_n (Figure 3). Figure 12 shows an example of this methodology for two surveys at $t_m=2012.6$ and $t_n=2017.7$. In both cases, we want to transform the horizontal coordinates estimated on these two dates to $t_i = 2011.0$, with the reference epoch at $t_0=2010.00$. Figure 13 shows the $DG\text{bM}$ surface displacement grids for each date.

To assess the reasonableness of the interpolation process used to derive the O-P displacement grids, we compare the grid values at the

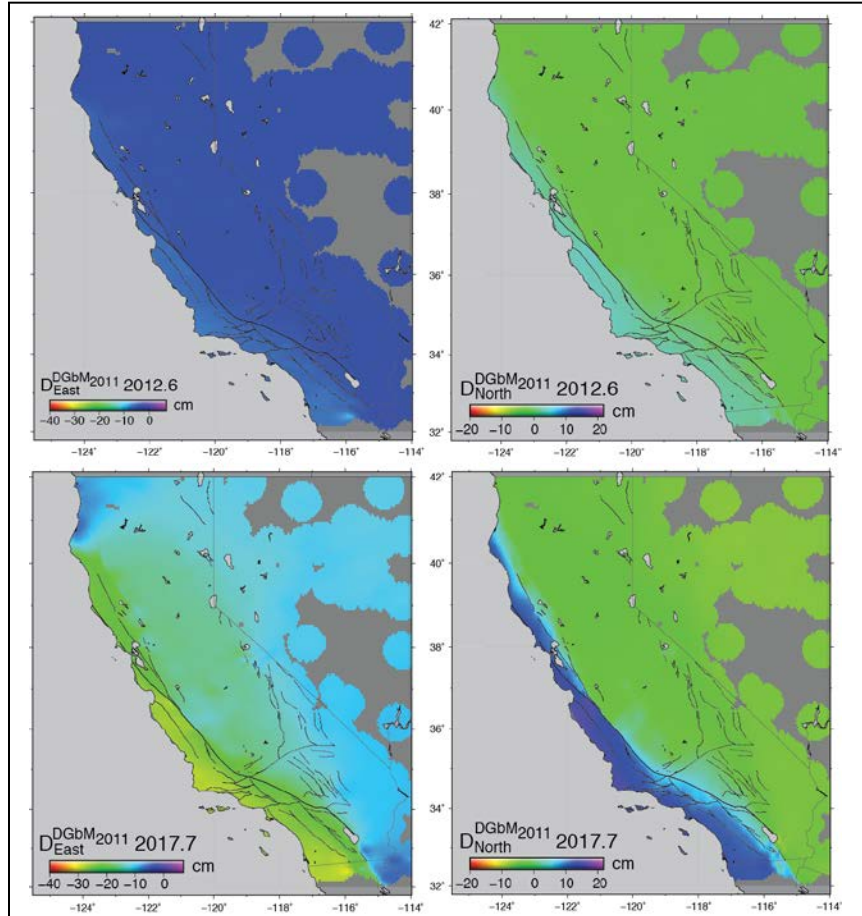


Figure 13. Observed Minus Predicted (O-P) DGbM displacement grids. (Upper panel) 2012.6 survey back to 2011.0. (Lower panel) 2017.7 survey back to 2011.0.

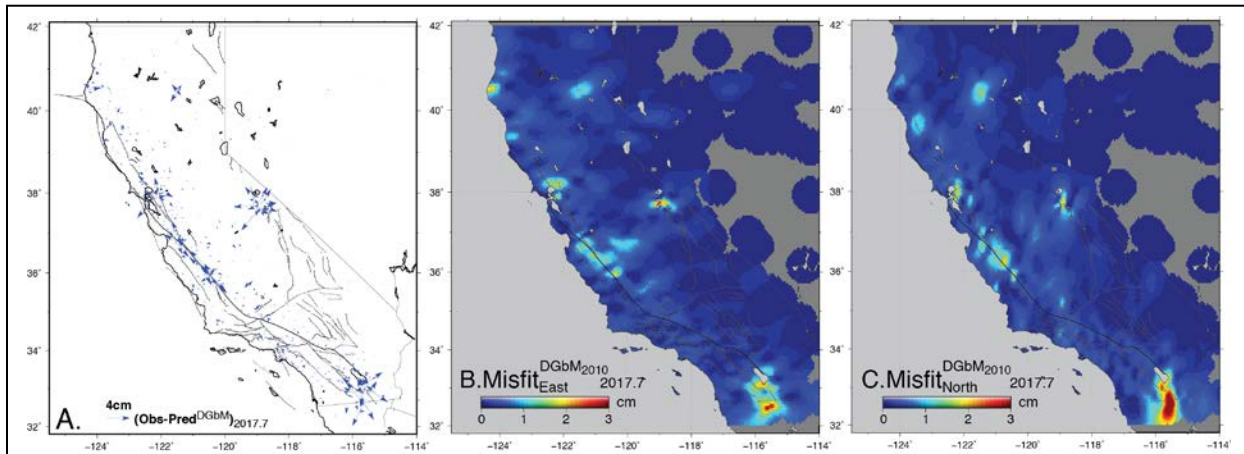
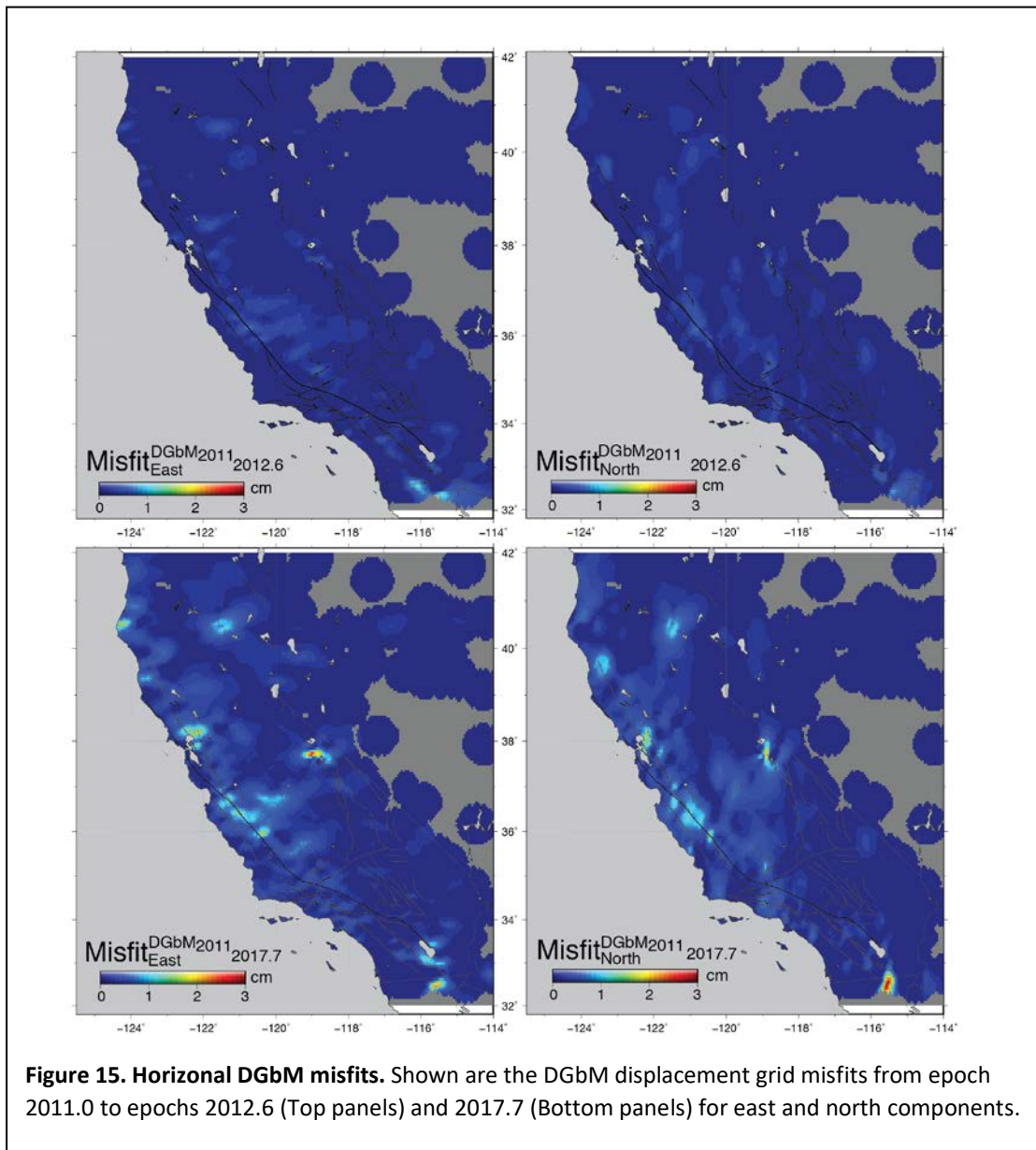


Figure 14: Misfits at the reference stations are the basis for the gridded interpolation misfits. A) Misfits between observations and DGbM at the epoch 2017.7 with reference date 2010.0. B) Misfits for the east component (cm) corresponding to the surface interpolation of absolute values of residuals shown in A. C) Same for the north component.

reference stations to the corresponding “true” observed values from the SOPAC processing (Figure 14). We refer to these as “point displacement misfits” and grid their absolute values to obtain the $DGBM_{2012.6}$ misfits at epoch 2012.6 and the $DGBM_{2017.7}$ misfits at epoch 2017.7, both with respect to epoch 2011.0 (Figure 15). The displacement misfits are smaller than 1 cm for the earlier date (2012.6) and mostly the same for the later date (2017.7). Exceptions at the later date are very small pockets of up to 2-3 cm due to residual postseismic effects for the 2010 Mw7.2 El Mayor-Cucapah and 2014 Mw6.1 Napa earthquakes (Table 1), the inflation of Long Valley caldera and the transition from the SAF to the Cascadia subduction zone in northern California. In these regions, very strong gradients and divergent motions are observed over small areas. It is instructive to display in Figure 16 the input O-P point displacements and the output O-P misfits from the gridding process at the reference stations (with respect to $t_0=2010.0$).



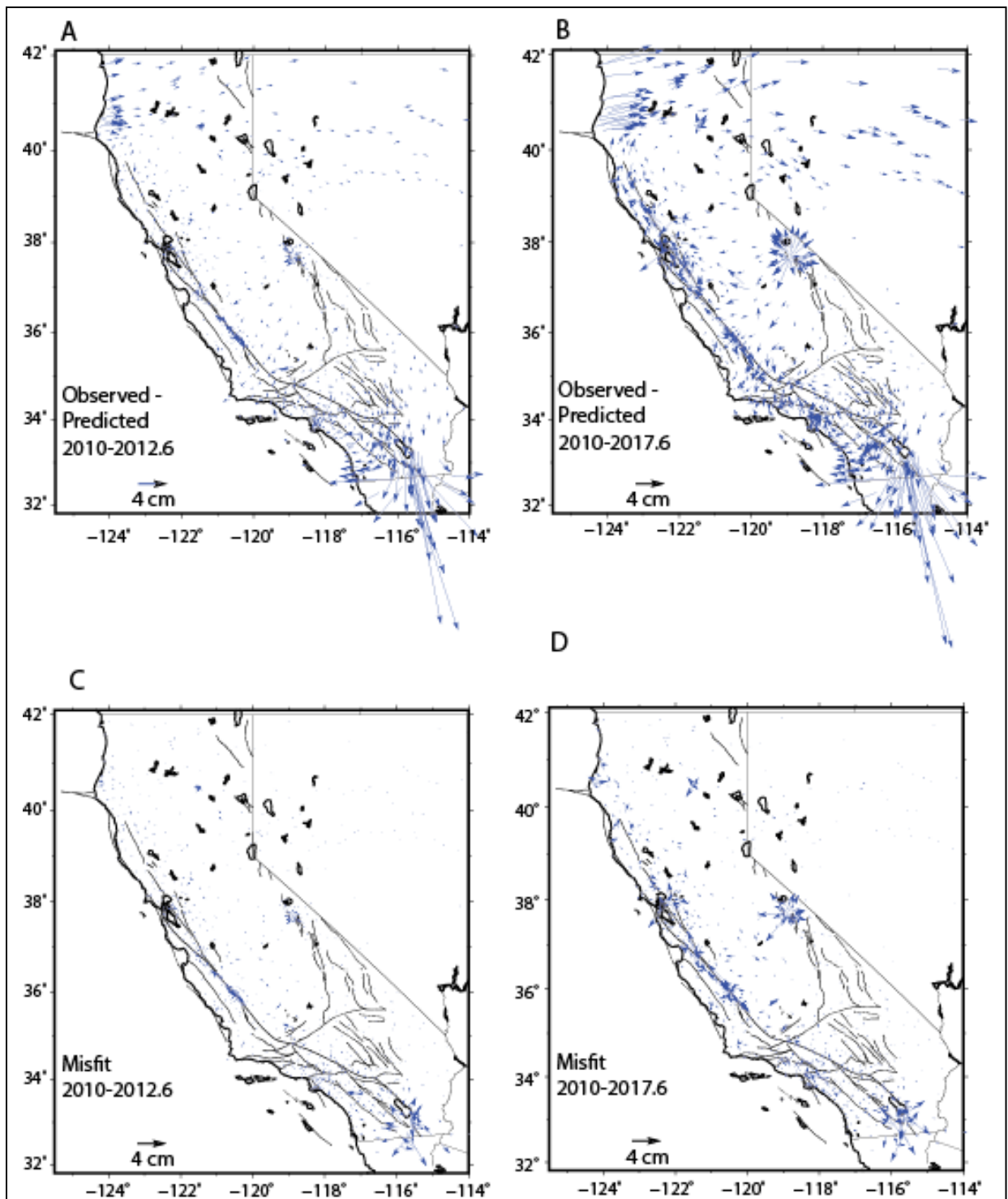


Figure 16. Misfits compared to O-P displacements. (A-B) Observed horizontal displacements minus displacement residuals predicted by Zeng and Shen (2017) for two dates with respect to 2010.0. (C-D) Misfit DGbM displacements. The misfits indicate that time-dependent processes have mostly been considered in the gridding process for the dynamic datum. As expected the misfits for the later date show larger values, for example, at the Long Valley Caldera, indicating limitations in interpolation.

Vertical datum

The vertical motions are considerably more erratic and often larger than the horizontal motions. Postseismic motion is smooth (Figure 4), while the effects of natural sources (e.g., climate, hydrology, drought, recharge) and anthropogenic effects (e.g., water and mineral withdrawal). Therefore, they are more difficult to model. For instance, vertical displacements in the Central Valley display numerous changes in slope related to drought, land use, water policy, etc. (Figures 17 and 18). Furthermore, the effects of tectonic processes only result in small vertical displacements throughout California, except for the coastal regions of northern California along the Cascadia subduction zone. Therefore, we do not use a geophysical or other model but simply interpolate the observed vertical displacements on a weekly basis. We call this the Dynamic Data-based Model approach (DDbM). The vertical O-P displacements and the grid misfits are shown in Figure 19, corresponding to the horizontal misfits in Figure 15.

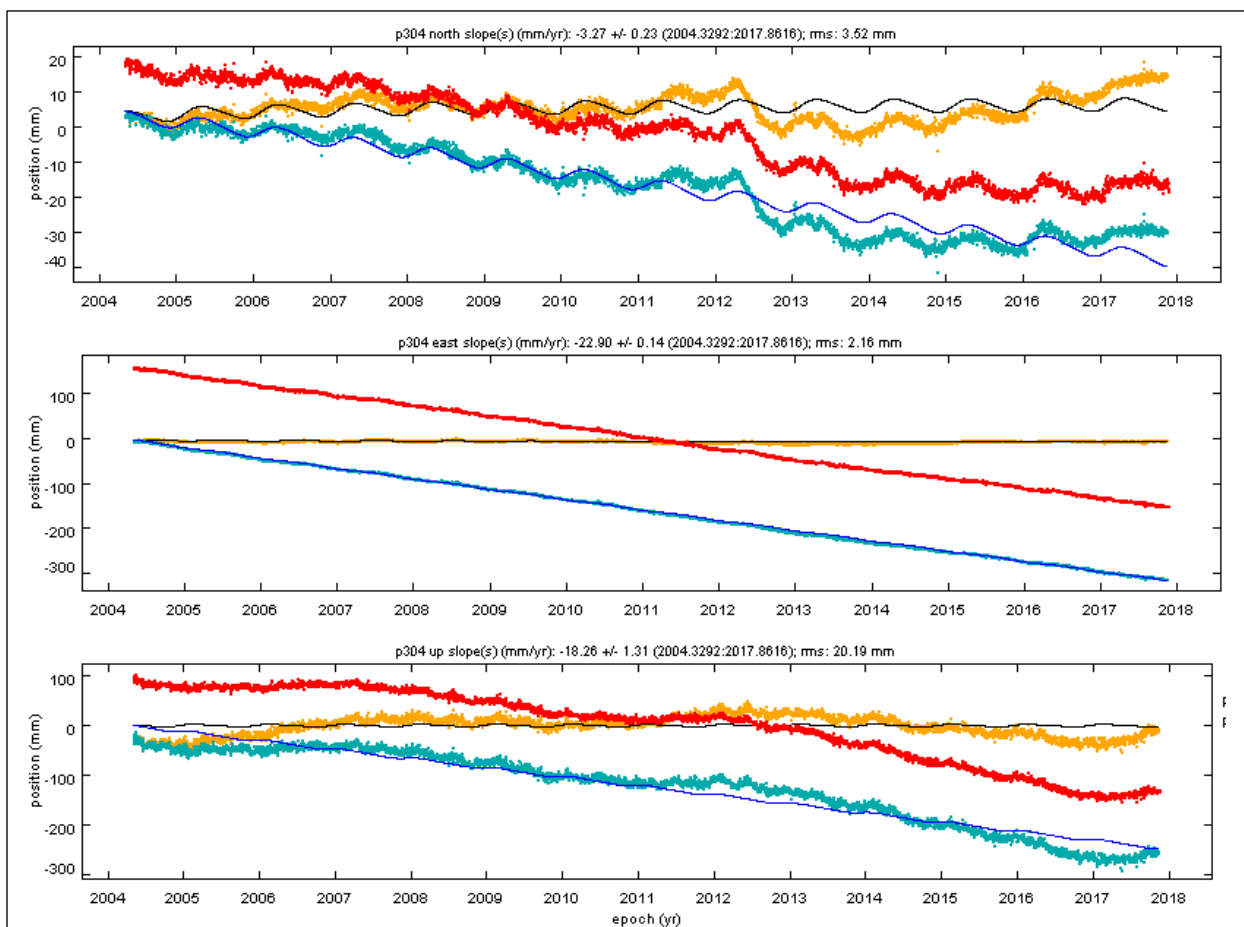
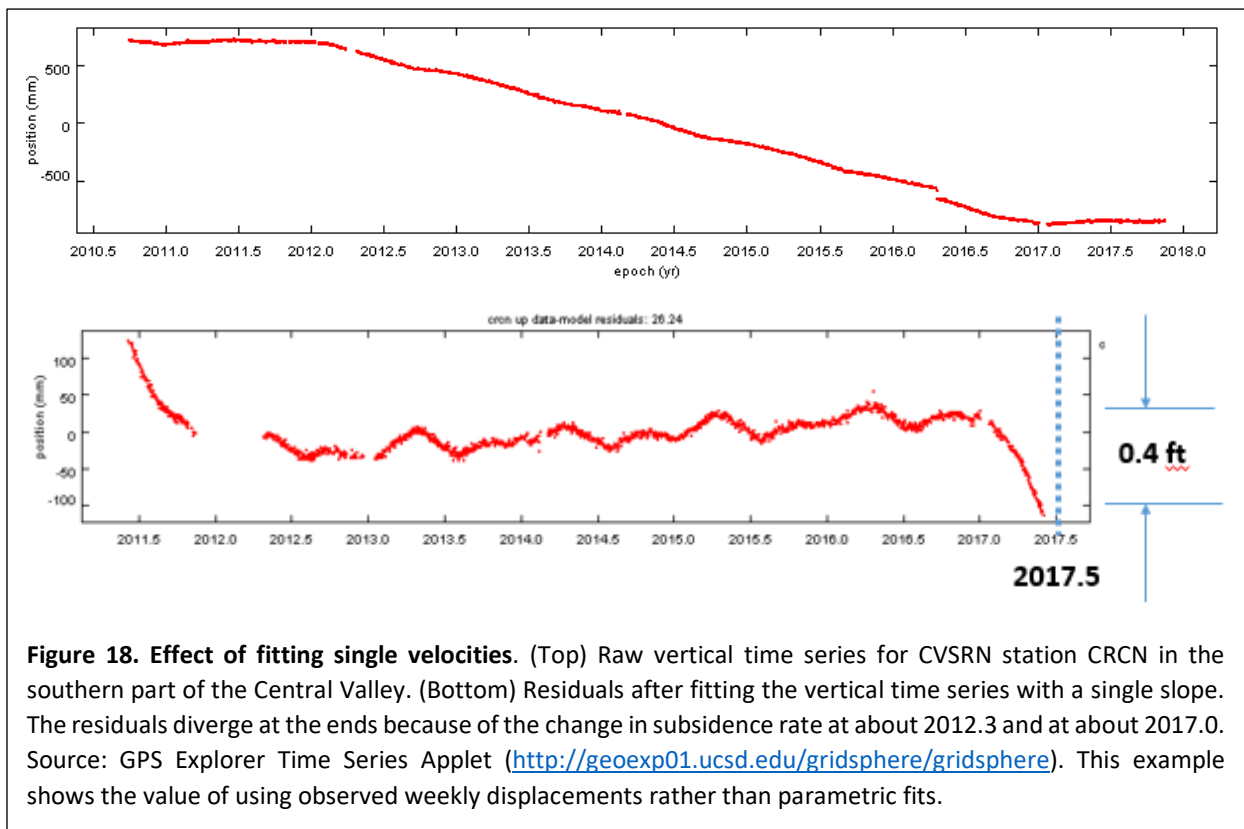


Figure 17. Variations in subsidence rates. Non-uniform subsidence at PBO station P304 near Mendota in the Central Valley of about 0.7 feet starting in 2007, leveling off in 2011, accelerated subsidence since 2012 due to drought conditions, and leveling off in 2017. The pattern of slope changes in the north component mirrors the pattern in the up component. The red lines indicate the raw displacements, the turquoise lines are the trended modeled displacements, the orange lines are the detrended displacements (the best-fitting slopes have been removed), blue lines are the trended traces and the black lines are the detrended traces. Source: GPS Explorer Time Series Applet (<http://geoexp01.ucsd.edu/gridsphere/gridsphere>).

For stations first appearing later than the reference date ($t_0=2010$, in our example), we proceed following a similar approach as explained earlier, predicting the station positions based on the previous DDbM grid. An insufficient density of stations and/or the absence of stations over several weeks may significantly impact the accuracy of the surface interpolation. In the Central Valley, there are only a dozen stations measuring the dramatic subsidence. If one of them stops recording over a few weeks, our methodology may underestimate the subsidence in the region and not be properly reflected in the misfits. There are two ways to tackle this issue. We can either use an accurate vertical motion model in the same way as a geophysical model or use the DGbM_t approach. For example, Snay et al. (2018) presented the TRANS4D model for vertical crustal velocities in Western CONUS. It is also possible to integrate denser observations such as less frequent InSAR measurements that will cover the whole area. The record of observed displacements at a sufficient number of GNSS stations can also be used to georeference the InSAR images.



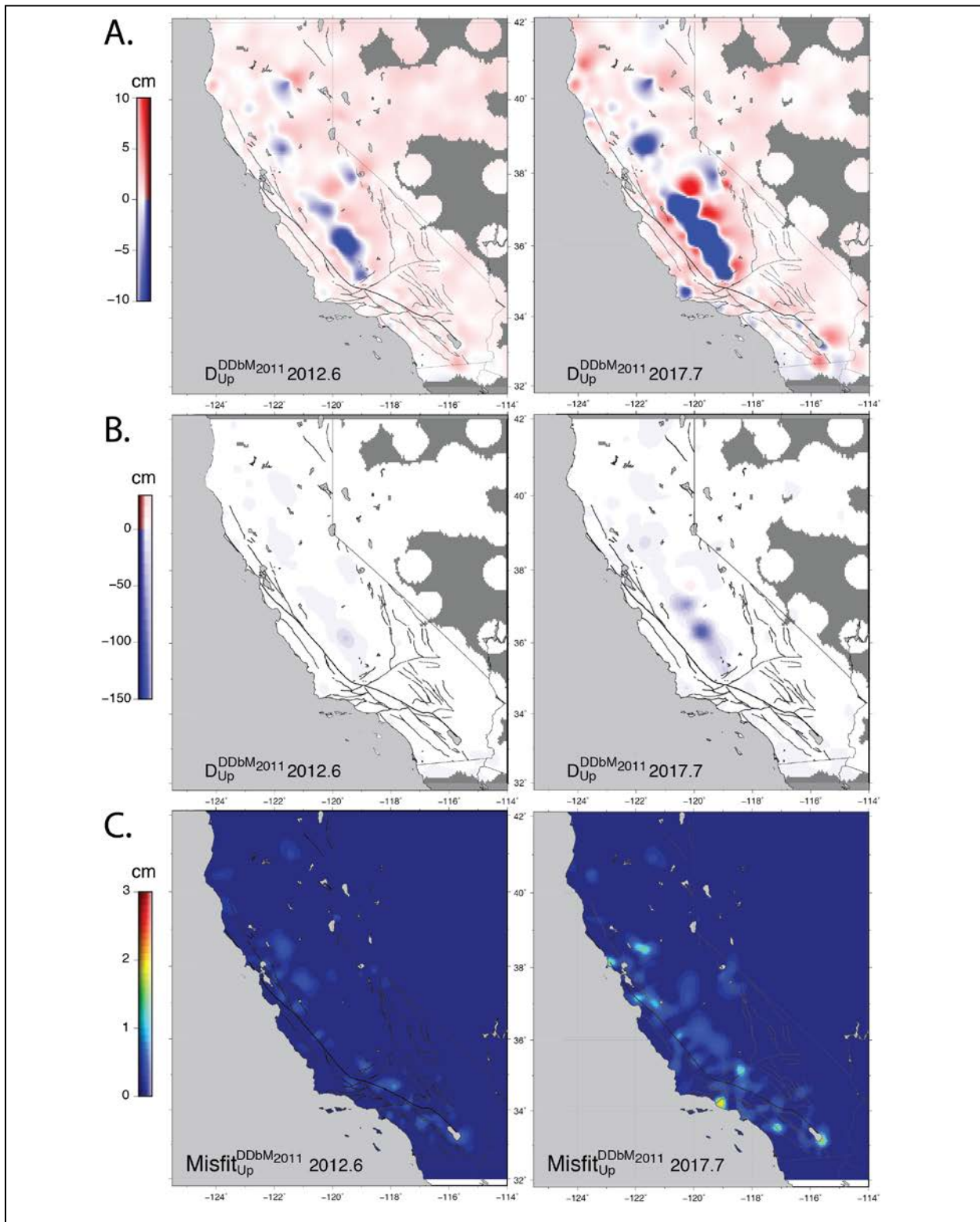


Figure 19. Vertical displacement interpolation and grid misfits. (A-B) Surface displacement grids (DDbM) at 2 different epochs with respect to 2011 (2012.6 – left panels, 2017.7 – right panels), shown at two color scales.

3. Discussion

Figure 20 provides a summary of the overall procedure for the horizontal dynamic datum – the procedure for the vertical is similar, except we use the DDbM approach instead of DGbM.

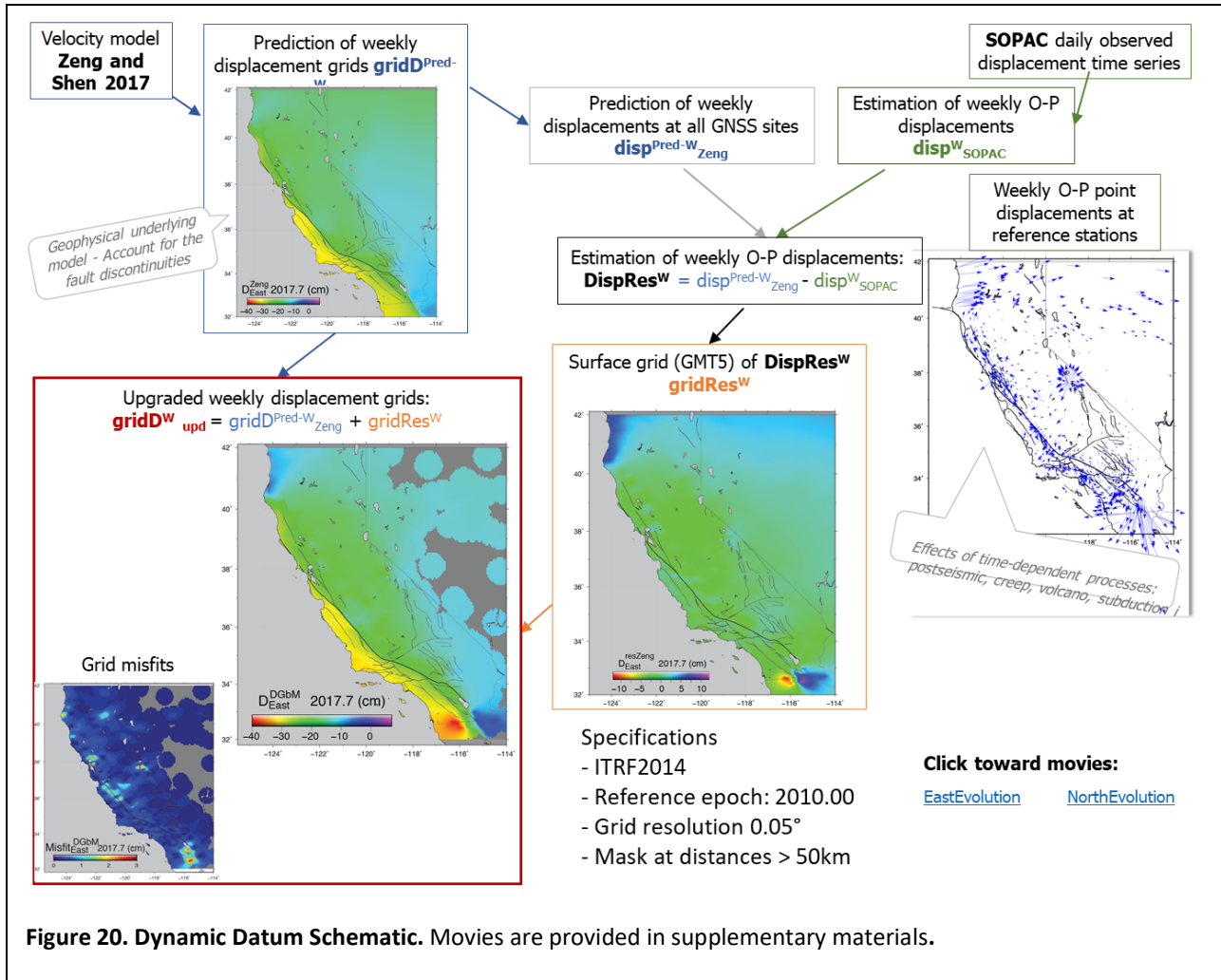


Figure 20. Dynamic Datum Schematic. Movies are provided in supplementary materials.

The two approaches for the horizontal, $DGbM_t$ and $DDbM_t$ produce consistent patterns overall, even for areas of significant postseismic deformation such as in southern California after the 2010 Mw7.2 El Mayor-Cucapah earthquake (Table 1). However, the use of an underlying geophysical model ($DGbM$) better reflects the discontinuities along the different fault segments, i.e., in areas of strong displacement gradients. The surface interpolation of GNSS displacement fields alone cannot reproduce them. For example, north of the Parkfield earthquake area (36°N), there is very sharp discontinuity where the fault is creeping, (Figure 6, profile *j*). Additionally, the amplitudes of interpolated displacement surfaces and misfits appear to be significantly larger without the geophysical model.

As stated earlier, the choice of geophysical model is somewhat subjective as most use similar fault locations and geometries – the choice of fault locking depths differs, as well as fault slip rates. Introduction of more realistic geophysical models that include the effects of postseismic deformation, through viscoelastic properties of the upper mantle (Figure 8 - e.g., Smith and Sandwell, 2006) and/or afterslip of

the fault surface (Freed, 2007) is desirable to better model the regions of strong divergent motion (Figure 16) but would not change our recommended dynamic datum methodology. Direct observations of precise (mm-level) point surface displacements from a dense GNSS network and complementary spatial InSAR data, where available, will always be the primary input for dynamic datums (and for geophysical models, i.e., to reduce the O-P residuals).

Infrequent coseismic displacements (Table 1) complicate the interpolation process since they will be distributed across the entire week in which they occur, but only in regions with significant offsets. This can be considered by splitting the affected weekly grid into two, one pre- and one post-earthquake.

Because of the irregular distribution of GNSS stations, as well as the addition and loss of stations over time, the quality of the surface interpolation will vary. To avoid the effect of sparse spatial coverage, we mask out areas that are located more than 50 km from the nearest stations. For California, the existing station coverage allows us to interpolate (grid) displacements reasonably well over the entire State; similarly, for Oregon and Washington State.

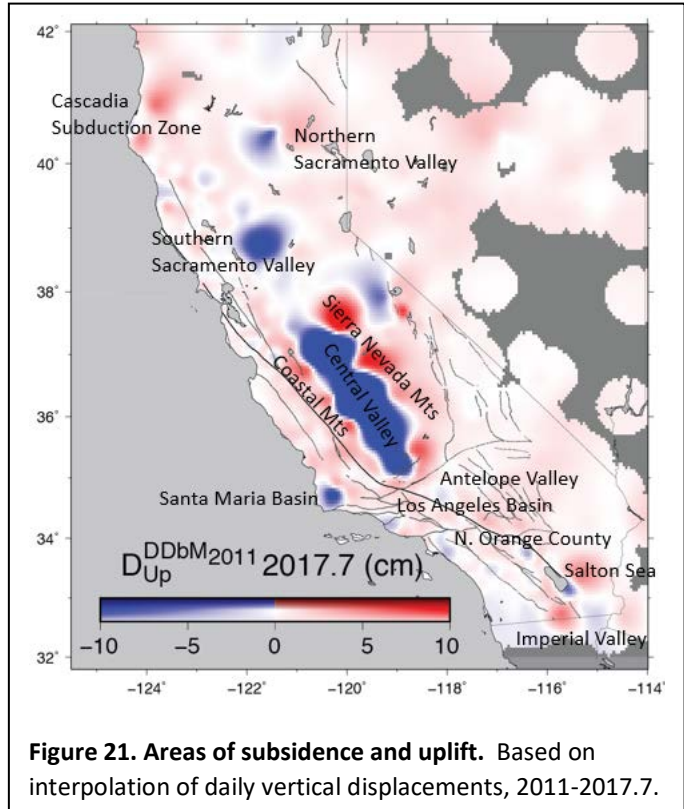


Figure 21. Areas of subsidence and uplift. Based on interpolation of daily vertical displacements, 2011-2017.7.

The vertical displacement grid is solely derived from weekly observations at the GNSS reference stations. Figure 21 highlights numerous areas of subsidence and uplift in California that have been well documented. Our dynamic datum approach deals well with vertical motions that are considerably more erratic than horizontal motions. The prototypical region is the Central Valley with numerous unpredictable changes in subsidence rates related to drought, land use, water policy, etc. (Figures 17 and 18). This is the main advantage of using weekly displacements rather than (possibly multiple) velocities for the dynamic datum.

4. Implementation

Our concept for implementing the dynamic datum consists of two related parts, one for post-processing and the second for real-time applications. For both, we make use of the stored weekly displacement grids (Figure 3). To transform coordinates between two arbitrary dates, t_n (the date of the survey) and t_m (an earlier date) at any location spanned by the reference stations, the corresponding grids are extracted from the database and differenced to obtain the grid corrections for the horizontal components:

$$\Delta DGbM_{n-m} = DGbM_n - DGbM_m$$

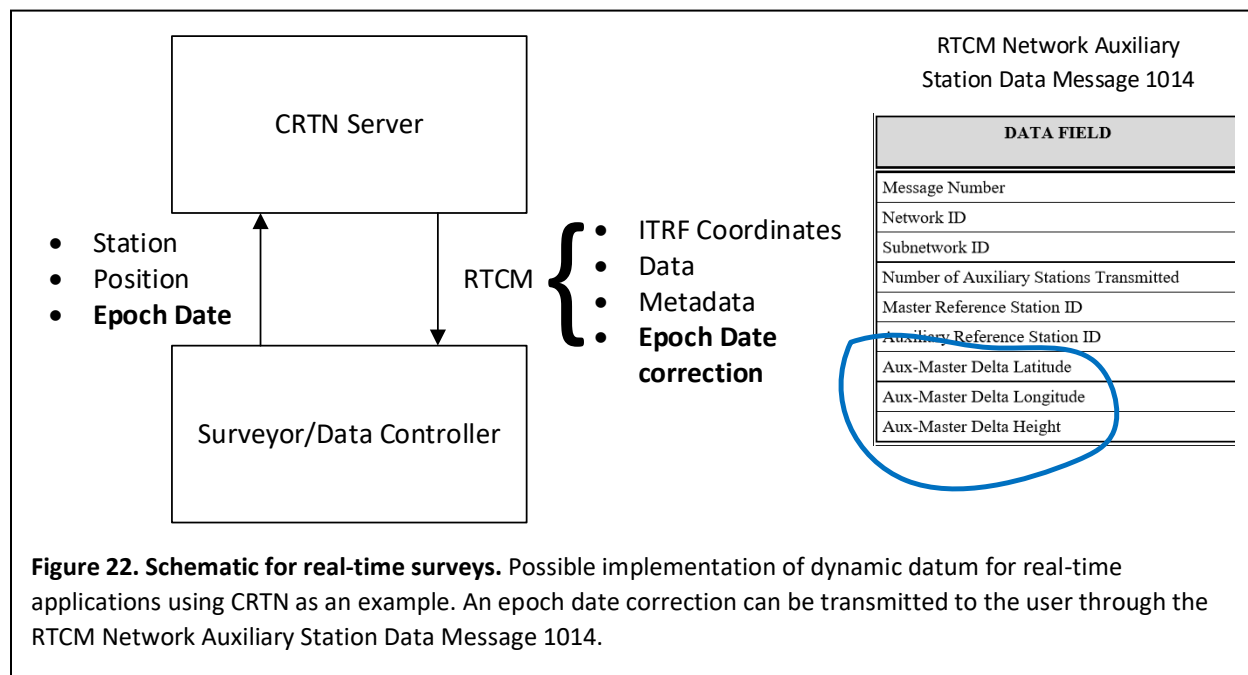
For the vertical component,

$$\Delta DDbM_{n-m} = DDbM_n - DDbM_m$$

Once the corrections are applied, the estimated coordinates are valid for the date m with respect to the same reference frame as at date n . In our methodology, positioning in the field (RTK – real-time kinematic surveying) or in post-processing should be performed in the ITRF (currently ITRF2014) to be consistent with the rapid or GNSS orbits provided by the International GNSS Service (IGS), as well as the broadcast ephemeris, and with the reference frame used by the operational center that produces the station displacements and stores the grid corrections. Once the ITRF coordinates of the station have been referred to the requested date, transformation to any other reference frame (e.g., NAD83(2011), state plane coordinates) can be performed.

4.1 Post-Processing

Access to the ITRF is available through SOPAC’s SECTOR utility (<http://sopac.ucsd.edu/sector.shtml>), which allows the transformation of California Spatial Reference Network coordinates from one date to another, but not for arbitrary locations within the State. This requires a new utility (let us call it SECTOR+), which performs the following: A user enters the coordinates of any surveyed station (in ITRF) within the region of the reference network, the date when the station was surveyed, and a date for the output coordinates. The output coordinates at the requested data can be with respect to another reference frame (e.g., NAD83(2011), as currently available in SECTOR).



4.2 Real-Time Surveying

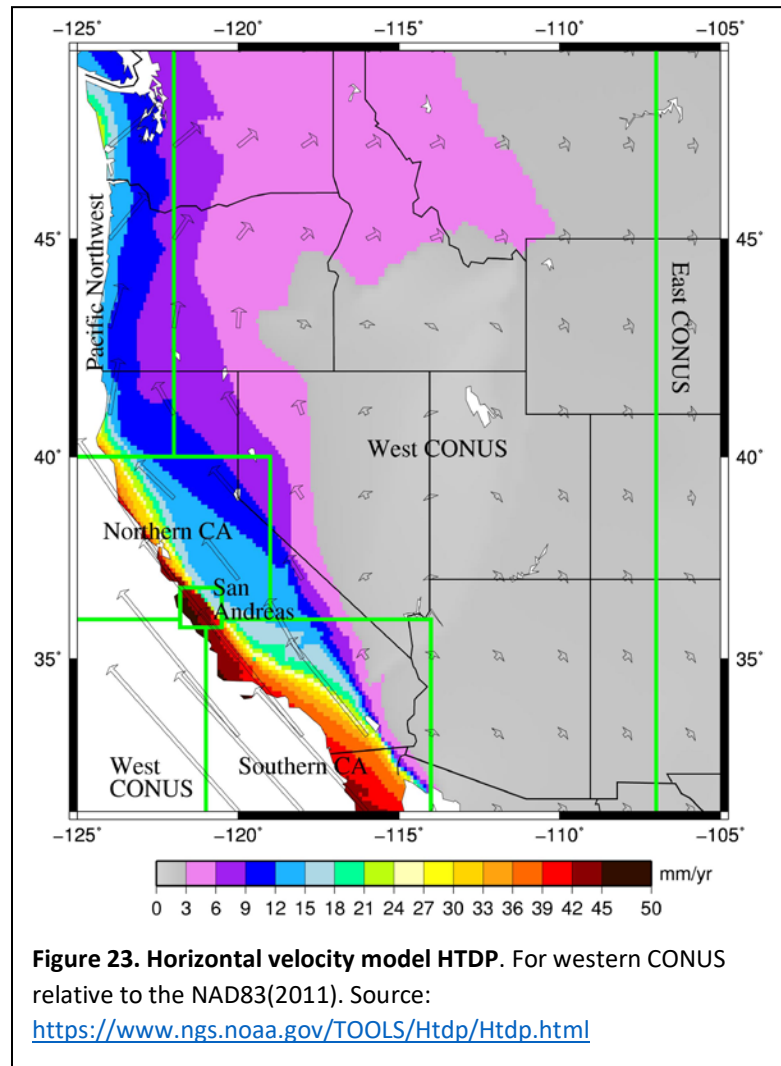
A method for obtaining transformed coordinates for RTK or network-mode positioning is illustrated in Figure 22. Using CRTN as an example, the normal RTK methodology is extended. In addition to the station NTRIP mount point and approximate position, the desired coordinate date is submitted to the CRTN server, where the SECTOR and SECTOR+ utilities are available in the background. As usual, the user is then supplied with the appropriate RTCM messages, the station metadata and the true-of-date ITRF coordinates of the reference stations, rather than NAD83(2011) coordinates, to be consistent with the GNSS and broadcast orbits. In addition, the dynamic datum corrections from the current date to the requested date are supplied. As indicated in Figure 22, this can be done using the existing RTCM auxiliary Station Data Message 1014, which contains three fields for latitude, longitude and height deltas. These

corrections are intended for network-mode surveying but can be applied to RTK surveys, as well. If one is performing network-mode surveys, one of the other special RTCM messages can be used to supply the dynamic datum correction. This approach requires the cooperation of the different manufacturers of survey data controllers and perhaps the receiver manufacturers, as well. It will require an outreach effort by CSRC stakeholders as described in the recommendations section below.

4.3 HTDP software

Task 1 is to “(1) Define the process and resources required to enhance the NGS modeling utility, Horizontal Time Dependent Positioning (HTDP), in collaboration with NGS, or to develop a new modeling utility for the geophysically complex area of California.” HTDP is based on a geophysical model that allows a user to transform horizontal coordinates across time and between spatial reference frames (Figure 23; Pearson et al., 2010; Pearson and Snay, 2013). In the context of our study, the long-term goal is to implement the dynamic models DGbM and DDbM across the intra-plate zone of western CONUS. This could be accomplished by upgrading HTDP or through an upgraded enhancement of DGbM and DDbM transportability to standard GIS and geospatial software.

The latest version of HTDP (3.25) is based on a simplified representation of the Earth’s crust that deforms as an elastic body. It considers secular station velocities obtained from several crustal motion velocity maps, and coseismic motions that occur during significant earthquakes (Table 1). For example, HTDP considers significant coseismic motions resulting from the 2010 Mw7.2 El Mayor-Cucapah earthquake in northwestern Baja California, Mexico, that significantly affected all cGNSS stations in southern California. However, the Earth’s crust also behaves as a viscoelastic body (Figure 8) as evidenced by postseismic deformation that can last more than a decade and result in accumulated motion of nearly the same magnitude as the instantaneous coseismic motion (Figure 4). HTDP does make accommodations for postseismic motion for selective earthquakes such as a model for the 2002 Mw7.9 Denali earthquake in Alaska (Pearson and Snay, 2013). However, HTDP is only periodically updated and it is unclear if it will continue to be maintained by the NGS. The methodology that we propose directly uses the weekly displacement observations to construct surface grids, so that new observations can be quickly



added without having to update the underlying geophysical model. The same comments hold true for the TRANS4D model for vertical crustal velocities in Western CONUS presented by Snay et al. (2018).

5. QA/QC Plan

We propose two QA/QC approaches. The first is an internal approach akin to a Monte Carlo algorithm. One reference station is chosen to serve as a survey station and is removed from the reference network. Dynamic data corrections are generated between some combination of epoch dates and the results compared to the known coordinates available through the SECTOR utility. This test is repeatedly conducted for other stations within both dense and sparse parts of the reference network and at the periphery of the network. This corresponds to a generalization of the grid misfit procedures (Figures 15 and 19).

The second approach is to work with volunteers who will review historical surveys or conduct new ones, comparing the dynamic datum corrections to normal procedures to relate true-of-date coordinates to Epoch Date coordinates, for example Epochs 2017.5 and 2011.00. Working with NGS, this could perhaps be accomplished through an OPUS Projects or OPUS Share Map interfaces, whereby GNSS campaign data are ingested into a QA/QC feedback loop (<https://www.ngs.noaa.gov/OPUS-Projects/OpusProjects.shtml>), or possibly through the NGS “GPS on Bench Mark” initiatives.

These two QA/QC approaches would provide input to considerations of the need for a supplemental Intra-Frame Velocity Model (IFVM) for the “Intra-Plate zones” as part of the NSRS implementation and maintenance, but leaves undefined how this might be developed, funded or implemented.

6. Recommendations

The dynamic datum concept is a somewhat radical departure from periodic publication of geodetic datums such as Epoch 2011.00 and Epoch 2017.50 (Bock et al., 2018) for deforming regions (<http://geoweb99.ucsd.edu/index.php/epoch2017/>; <http://geoweb99.ucsd.edu/index.php/previous-datums/>). However, both approaches rely upon daily displacement observations by a network of cGNSS reference stations, such as the CSRN and its CRTN subset.

Potential collaborative partners and stakeholders are those that require precise cm-level surveying and spatial referencing for geographic information systems (GIS). An important source is the report “Maintaining California’s Geodetic Control System Strategic Assessment” by the Geodetic Control Working Group (Martin et al., 2007). The report has been endorsed by the League of California Surveying Organizations (LCSO), County Engineers Association of California (CEAC), American Council of Engineering Companies California (ACEC), California’s Land Surveyor’s Association (CLSA), Urban and Regional Information Systems Association (URISA) and Esri. Other organizations are represented in the CSRC Coordinating Council (<http://geoweb99.ucsd.edu/index.php/coordinating-council/>). It is critical to reinvigorate the Council to garner support for the dynamic datum and the CSRC, in general. The dynamic datum concept can be implemented for users of real-time GNSS networks such as the California Real Time Network (CRTN), Pacific Northwest Geodetic Array (PANGA) and Oregon Real-time GPS Network (ORGN), with several thousand active users, and the Caltrans internal real-time networks (Central Valley, San Diego County). Buy in by private real-time networks is a possibility but is unlikely since they operate their own reference stations, which are not tied into the CSRS. Nevertheless, a utility that provides coordinates for any location in California at a specific time could be useful to these users, as well, so it is worthwhile

pursuing these contacts. As mentioned in section 3, it is important to obtain cooperation and/or support from manufacturers of field data recorders and geodetic-quality GNSS receivers.

One option for funding the development and maintenance of the dynamic datum and its required analysis infrastructure is through State funding along the lines of the recommendations of the Geodetic Control Working Group (Martin et al., 2007). An option to partially fund the maintenance of the dynamic datum is through an expanded CRTN Consortium and contributing membership. The funding for the development of the dynamic datum could be matched by the NGS through university engagement and/or collaboration with Caltrans and the CSRC. For example, this could involve rapid upgrade and maintenance of the HTDP software to fulfill the NGS mission requirements, specifically with respect to reference frames. It is envisaged that support for such an effort would require a Pilot Project with NGS. The outcome would certainly be of interest to stakeholders throughout Western CONUS, including Oregon and Washington State and would provide the tie to NATRF 2022 and NAPGD 2022.

Acknowledgments

We strongly appreciate the support of Caltrans, the Office of Land Surveys, Contract Manager Mark S. Turner and Task Order Manager Scott P. Martin. Both have the vision to evaluate the feasibility of a dynamic datum for California. Essential input and support by the NGS Pacific Southwest Regional Advisor, Dana J. Caccamise II is much appreciated. Greg Helmer provided a careful review. SOPAC staff maintain our archive and analysis systems, including Peng Fang and Anne Sullivan. Support for Emilie Klein is also provided by NASA grant NNX17AD99G. SOPAC data archive and analysis infrastructure leveraged for this project were made possible by NASA grant NNX13AI45A-001 and National Science Foundation grant EAR-1400901.

References

- Amos, C. B., P. Audet, W. C. Hammond, R. Bürgmann, I. A. Johanson and G. Blewitt (2014), Uplift and seismicity driven by groundwater depletion in central California, *Nature*, 509(7501), 483-486.
- Argus, D. F., Y. Fu and F. W. Landerer (2014), Seasonal variation in total water storage in California inferred from GPS observations of vertical land motion, *Geophysical Research Letters*, 41(6), 1971-1980.
- Bawden, G. W., W. Thatcher, R. S. Stein, K. W. Hudnut and G. Peltzer (2001), Tectonic contraction across Los Angeles after removal of groundwater pumping effects, *Nature* 412(6849), 812-815.
- Bock, Y. and D. Melgar (2016), Physical Applications of GPS Geodesy: A Review, *Rep. Prog. Phys.* 79, 10, doi:10.1088/0034-4885/79/10/106801.
- Bock, Y., S. Kedar, A. W. Moore, P. Fang, J. Geng, Z. Liu, D. Melgar, S. E. Owen, M. B. Squibb, F. Webb (2016), Twenty-Two Years of Combined GPS Products for Geophysical Applications and a Decade of Seismogeodesy, International Association of Geodesy Symposia, Springer International Publishing, doi:10.1007/1345_2016_220.
- Bock, Y., P. Fang and G. R. Helmer (2018), California Spatial Reference System: CSRS Epoch 2017.50 (NAD83), Report to California Department of Transportation (Caltrans), January 4.
- Borsa, A. A., D. C. Agnew and D. R. Cayan (2014). Ongoing drought-induced uplift in the western United States, *Science*, 345(6204), 1587-1590.
- Freed, A. M. (2007), Afterslip (and only afterslip) following the 2004 Parkfield, California, earthquake, *Geophysical Research Letters*, 34.
- King, N., D. Argus, J. Langbein, D. Agnew, G. Bawden, R. Dollar, Z. Liu, D. Galloway, E. Reichard and A. Yong (2007), Space geodetic observation of expansion of the San Gabriel Valley, California, aquifer system, during heavy rainfall in winter 2004–2005, *Journal of Geophysical Research: Solid Earth*, 112(B3), 1978-2012.
- Martin, S. L., L. Blake, J. Canas, T. Dougherty, K. Hart, J. Height, R. Hunsicker, B. Joffe, N. King, M. McGee, R. Moore, R. Parks and M. S. Turner (2017), "Maintaining California's Geodetic Control System Strategic Assessment," California GIS Council's Geodetic Control Work Group
- Nikolaidis, R. (2002), Observation of geodetic and seismic deformation with the Global Positioning System. La Jolla, California, PhD thesis, University of California San Diego.
- NGS (2017), NOAA Technical Report NOS NGS 62, Blueprint for 2022, Part 1 Geometric Coordinates, https://geodesy.noaa.gov/PUBS_LIB/NOAA_TR_NOS_NGS_0062.pdf
- Pearson, C., R. McCaffrey, J. L. Elliott, and R. Snay (2010), HTDP 3.0: Software for coping with the coordinate changes associated with crustal motion, *Journal of Surveying Engineering*, doi: 10.1061/(ASCE)SU.1943-5428.0000013. <https://www.ngs.noaa.gov/TOOLS/Htdp/PearsonetalJSE2010.pdf>
- Pearson, C. and R. Snay (2012), Introducing HTDP 3.1 to transform coordinates across time and spatial reference frames. *GPS Solutions*, doi:10.1007/s10291-012-0255-y. https://www.ngs.noaa.gov/TOOLS/Htdp/Pearson_Snay_2012.pdf

Sandwell, D. T., and P. Wessel (2016), Interpolation of 2-D vector data using constraints from elasticity, *Geophysical Research Letters*, 43, doi:10.1002/2016GL070340.

Shen, Z.-K., D. D. Jackson, Y. Feng, M. Cline, M. Kim, P. Fang and Y. Bock (1994), Postseismic deformation following the Landers earthquake, California, 28 June 1992. *Bulletin of the Seismological Society of America*, 84(3): 780-791.

Smith, B.R. and Sandwell, D.T. (2006), A model of the earthquake cycle along the San Andreas Fault System for the past 1000 years, *Journal of Geophysical Research: Solid Earth*, 111(B1).

Snay R. A., J. Saleh, C. F. Pearson (2008), Improving TRANS4D's model for vertical crustal velocities in Western CONUS, *Journal of Applied Geodesy*, <https://doi.org/10.1515/jag-2018-0010>.

Tong, X, DT Sandwell, and B Smith-Konter (2013), High-resolution interseismic velocity data along the San Andreas Fault from GPS and InSAR¹, *Journal of Geophysical Research: Solid Earth*: 1-21.

Williams, S. (2003), the effect of coloured noise on the uncertainties of rates estimated from geodetic time series, *Journal of Geodesy*, 76(9-10), 483-494.

Zeng, Y. and Shen, Z. K. (2017), A Fault-Based Model for Crustal Deformation in the Western United States Based on a Combined Inversion of GPS and Geologic Inputs, *Bulletin of the Seismological Society of America*, 107(6), 2597-2612.

Zhang, J. (1996), Continuous GPS measurements of crustal deformation in southern California, PhD thesis, University of California, San Diego.

Displacement Grid Movies

(1) **de_totMask_June6.gif**

DGbM displacement grid, east component 2010.0—2017.9

(2) **dn_totMask_June6.gif**

DGbM displacement grid, north component 2010.0—2017.9

(3) **du_drought_totMask_June6.gif**

DDbM displacement grid, vertical component, large-scale motions 2010.0—2017.9

(4) **du_season_totMask_June6.gif**

DDbM displacement grid, vertical component, small-scale motions 2010.0—2017.9

List of Acronyms

ACEC	American Council of Engineering Companies California
Caltrans	California Department of Transportation
CEAC	County Engineers Association of California
CLSA	California’s Land Surveyor’s Association
CONUS	Continental United States
CRTN	California Real Time Network
CSRC	California Spatial Reference Center
CSRN	California Spatial Reference Network
CSRS	California Spatial Reference System
CSRS Epoch 2017.50 (NAD83)	Epoch 2017.50
DDbM	Dynamic Data-based Model grid
DGbM	Dynamic Geophysical-based Model grid
GCWG	Geodetic Control Working Group
GIS	Geographic Information System
GMT	Generic Mapping Tools
HTDP	Horizontal Time Dependent Positioning
IGS	International GNSS Service

InSAR	Interferometric Synthetic Aperture Radar
ITRF	International Terrestrial Reference Frame
JPL	Jet Propulsion Laboratory
LCSO	League of California Surveying Organizations
NAD83	North America Datum 1983
NAPGD 2022	North American-Pacific Geopotential Datum of 2022
NATRF 2022	North American Terrestrial Reference Frame of 2022
NGS	(NOAA/NOS) National Geodetic Survey
NSRS	National Spatial Reference System
O-P	Observed minus Predicted
OPUS	NGS Online Positioning User Service
ORGN	Oregon Real-Time GNSS Network
PANGA	Pacific Northwest Geodetic Array
RTK	Real-Time Kinematic surveying
SECTOR	Scripps Epoch Coordinate Tool and Online Resource
SIO	Scripps Institution of Oceanography
TRANS4D	Transformations in Four Dimensions
URISA	Urban and Regional Information Systems Association